DEVELOPMENT OF A DROSOPHILA CMT MODEL VIA OVEREXPRESSION AND KNOCKING-IN OF GDAP1 GENE

by

Hüseyin Kaya Akyüz

B.S., Molecular Biology and Genetics, Boğaziçi University, 2011

Submitted to the Institute for Graduate Studies in
Science and Engineering in partial fulfillment of
the requirements for the degree of
Master of Science

Graduate Program in Molecular Biology and Genetics
Boğaziçi University

2013

To my mother...

ACKNOWLEDGEMENTS

I would like to thank my co-supervisors Prof. Esra Battaloğlu and Assoc. Prof. Arzu Çelik for passing on their knowledge and expertise, allowing me to improve myself and learn from my mistakes. Through my master's degree, I have learned greatly and increased my capacity as a graduate student with their assistance.

I would like to thank my jury members, Prof. Hande Çağlayan, Prof. Arzu Karabay Korkmaz and Assist. Prof. Necla Birgül-İyison, who took their most valuable time to read my thesis. It is an honor to receive feedback from them about my work.

I would also like to thank all of my friends, who have been with me in my most joyful and distressed times. Being a scientist makes it necessary to accept challenges and the support of my friends have been vital in keeping me on the right track while I was trying to cope with my problems; they have made life more enjoyable: Kerem, Merve K., Duygu D., Burçak, Merve S., Cansu, Begüm, Büşra, Alperen, Duygu K., Gamze, Ece, Bahar, Selen, Kaan, Aslı, Neslihan, Yıldız, Emirhan, Özden, Burcu, Özge, Esra, Müge, Salih, İlker, Ayten and Banu.

Finally, I would like to thank my dad, sister and brother for being there for me in the most difficult and pleasant times. I would like to thank my uncle Prof. Ali Akyüz especially for his guidance and encouraging me to pursue a career in science.

Lastly, I would like to acknowledge the Scientific and Technological Research Council of Turkey (TÜBİTAK) for supporting me and this project (TBAG 112T275).

ABSTRACT

DEVELOPMENT OF A DROSOPHILA CMT MODEL VIA OVEREXPRESSION AND KNOCKING-IN OF GDAP1 GENE

Charcot-Marie-Tooth (CMT) disease is one of the most common inherited disorders of the nervous system. Known also as hereditary motor and sensory neuropathy, this disease is characterized by distal sensory loss, muscle weakness and atrophy, loss of deep tendon reflexes and skeletal deformities, especially in the lower extremities. However, genetically, it is a highly heterogeneous disease, with mutations in approximately 40 genes associated with the disease. *GDAP1* is one of the most frequently mutated genes among recessively inherited CMT though it also exhibits dominant segregation. As its mutations may cause demyelinating, axonal and intermediate subtypes of the disease and mostly severe and early onset neuropathy, it is an important candidate to study. In the scope of this research, we have aimed to develop a *Drosophila* CMT model using overexpression of its ortholog in flies and generation of various knock-in constructs. The second aim of this study is to understand the functions of GDAP1, which is a mitochondrial fission factor with glutathione S-transferase activity, and CG4623 that is an uncharacterized protein. In the first part of the study, tools have been generated for integrase-mediated approach for gene knock-out. Among these are constructs for knocking-in human *GDAP1* and CMT-causing nine mutant forms of *GDAP1* in place of its *Drosophila* homolog (*CG4623*), a GAL4 driver and an mCherry reporter for *CG4623*. Along with these, the initial steps of anti-CG4623 antibody production have been taken. In the second part of the project, a fly line overexpressing *CG4623* under UAS control has been generated in order to understand the function of this gene and to compare it to its ortholog in humans. Lastly, available mutant lines for mitochondrial dynamics-related genes have been used in analyses of longevity and mitochondrial dynamics, which may be adapted for analyses of the knock-in and overexpression lines. With this study, our final goal is to shed light on the pathogenesis of CMT through understanding the function of *GDAP1* and its role in neuropathy by starting the fly model for the disease in our laboratory.

ÖZET

GDAP1 GENİNİN YÜKSEK ANLATIMI VE KNOCK-IN YÖNTEMİYLE DROSOPHİLA CMT MODELİNİN OLUŞTURULMASI

Charcot-Marie-Tooth (CMT) en sık görülen kalıtsal sinir sistemi hastalıklarından biridir. Kalıtsal motor ve duysal nöropati olarak da bilinen bu hastalık distal duysal kayıp, kas güçlüğü ve atrofi, derin tendon reflekslerinin kaybı ve özellikle alt ekstremitelerde iskelet bozukluklarıyla ayırt edilmektedir. Ancak genetik açıdan çok heterojen bir hastalıktır ve yaklaşık 40 gen bu hastalıkla ilişkilendirilmiştir. Baskın kalıtım da göstermesinin yanında, çekinik kalıtılan CMT içerisinde en sık mutasyon görülen genlerden biri *GDAP1'*dir. Mutasyonlarının, hastalığın demiyelizan, aksonal ve ara tiplerine ve çoğunlukla şiddetli ve erken başlangıçlı nöropatiye sebep olması, bu geni moleküler çalışmalar için önemli bir aday yapmaktadır. Bu araştırma çerçevesinde, *GDAP1*'in sinekteki homoloğu *CG4623*'ün yüksek anlatımı ve *CG4623* yerine yerleştirilebilecek yapıların oluşturulması ile *Drosophila* CMT modeli geliştirmeyi amaçladık. Araştırmanın ikinci amacı glutatyon S-transferaz aktivitesine sahip mitokondriyal fizyon faktörü olan GDAP1 ve karakterize edilmemiş CG4623 proteinlerinin işlevlerini anlamaktır. Araştırmanın ilk kısmında integraz aracılığıyla gen silme yöntemi için araçlar geliştirilmiştir. Oluşturulan araçlar arasında *Drosophila* homoloğunun (*CG4623*) yerine yerleştirmek üzere *GDAP1* ve *GDAP1*'in CMT'ye sebep olan dokuz mutant formu için yapılar, bir GAL4 yükselticisi ve *CG4623* için mCherry raportörü bulunmaktadır. Bunların yanında, anti-CG4623 antikorunu üretmek için gerekli moleküler yapılar da oluşturulmuştur. Çalışmanın ikinci kısmında, CG4623 geninin işlevini anlamak ve insandaki ortoloğuyla karşılaştırmak üzere UAS kontrolü altında bu geni yüksek anlatan bir sinek hattı geliştirilmiştir. Son olarak, mitokondriyal dinamikler ile ilgili genlerin mevcut mutant hatları kullanılarak yaşam süresi ve mitokondriyal dinamiklerin analizleri gerçekleştirilmiştir. Bu analizlerin ileride knock-in ve yüksek anlatım hatlarında uygulanabilir olması için ortam hazırlanmıştır. Bu araştırmayla, nihai amacımız, CMT hastalığının sinek modelinin oluşturulması çalışmalarını laboratuvarımızda başlatarak GDAP1'in işlevi ve nöropatideki rolünü incelemek ve böylece hastalığın oluşumu ve gelişimine ışık tutmaktır.

TABLE OF CONTENTS

LIST OF FIGURES

LIST OF TABLES

LIST OF SYMBOLS

R	arginine
D	aspartate
C	cysteine
E	glutamate
Q	glutamine
G	glycine
L	leucine
m	meter
M	methionine
mV	millivolt
P	proline
s	second
S	serine
W	tryptophan
Y	tyrosine
v	volume
w	weight
α	alpha
µg	microgram
µl	microliter
Φ	phi

LIST OF ACRONYMS/ABBREVIATIONS

AX	axonal
bp	basepair
CNS	central nervous system
CMT	Charcot-Marie-Tooth disease
CMAP	compound motor action potential
DM	demyelinating
DNA	deoxyribonucleic acid
Dom	dominant
GDAP1	Ganglioside-induced differentiation-associated protein 1
GDAP1L1	Ganglioside-induced differentiation-associated protein 1 like 1
GSH	glutathione
GST	glutathione S-transferase
GFP	green fluorescent protein
GTP	guanosine triphosphate
HMSN	hereditary motor and sensory neuropathy
HD	hydrophobic domain
IE	inexcitable
IMAGO	integrase-mediated approach for gene knock-out
INT	intermediate
kb	kilobase
kD	kilodalton
mNCV	motor nerve conduction velocity
NCBI	National Center for Biotechnology Information
NC	negative control
ND	not determined
PNS	peripheral nervous system
ROS	reactive oxygen species
Rec	recessive
RMCE	recombinase mediated cassette exchange
RFP	red fluorescent protein

RD	restriction digestion
RNA	ribonucleic acid
RNAi	ribonucleic acid interference
TM	transmembrane domain
UAS	upstream activating sequence
WI	walking independently
WS	walking with support
WB	wheelchair bound

1. INTRODUCTION

Charcot-Marie-Tooth disease (CMT) is one of the most common inherited disorders of the peripheral nervous system (PNS). CMT is also known as Hereditary Motor and Sensory Neuropathy (HMSN) as it affects both motor and sensory neurons. The prevalence of the disease changes according to geographical location and is reported to be 8-41 per 100.000 individuals (Martyn & Hughes, 1997). Even though CMT is a heterogeneous disease, clinicians characterize it noting several slowly progressing key features: distal sensory loss, weakness, muscle atrophy, loss of deep tendon reflexes and skeletal deformities, especially in the lower extremities (Harding & Thomas, 1980). Although in 60% of the cases, symptoms arise in the first decade, the onset and progression of the disease depends on patient's genetic makeup (Vallat, Mathis, & Funalot, 2013).

The disease is categorized into two major groups according to electrophysiological features: demyelinating (CMT1), and axonal forms (CMT2), where motor nerve conduction velocities (mNCV) are uniformly slow (below 38 m/s for median nerve) and normal or slightly reduced, respectively. The intermediate form of the disease presents mNCV of 25 to 45 m/s and exhibits features of both demyelinating and axonal neuropathy. Compared to CMT1 cases, CMT2 patients generally have compound motor action potential (CMAP) of lower amplitudes (Zuchner & Vance, 2006). The electrophysiological findings are supported with histopathology, where demyelination and onion bulb formations are observed for CMT1 and axonal loss is evident in CMT2.

Although 90% of all genetically identifiable CMT cases are caused by mutations in only four genes (*PMP22*, *GJB1*, *MPZ*, *MFN2*), approximately 40 genes have been associated with CMT and there are still a number of loci associated with the disease, for which specific genes have not yet been identified (Figure 1.1) (Siskind *et al*., 2013; Vallat *et al*., 2013). The most common mutation found in CMT patients is the duplication of a 1.4 Mb region on chromosome 17p.11.2, including the *peripheral myelin protein 22* (*PMP22*), which is the causative mutation for 70.7% of all CMT1 cases (Lupski *et al*., 1991; Nelis *et al*., 1996).

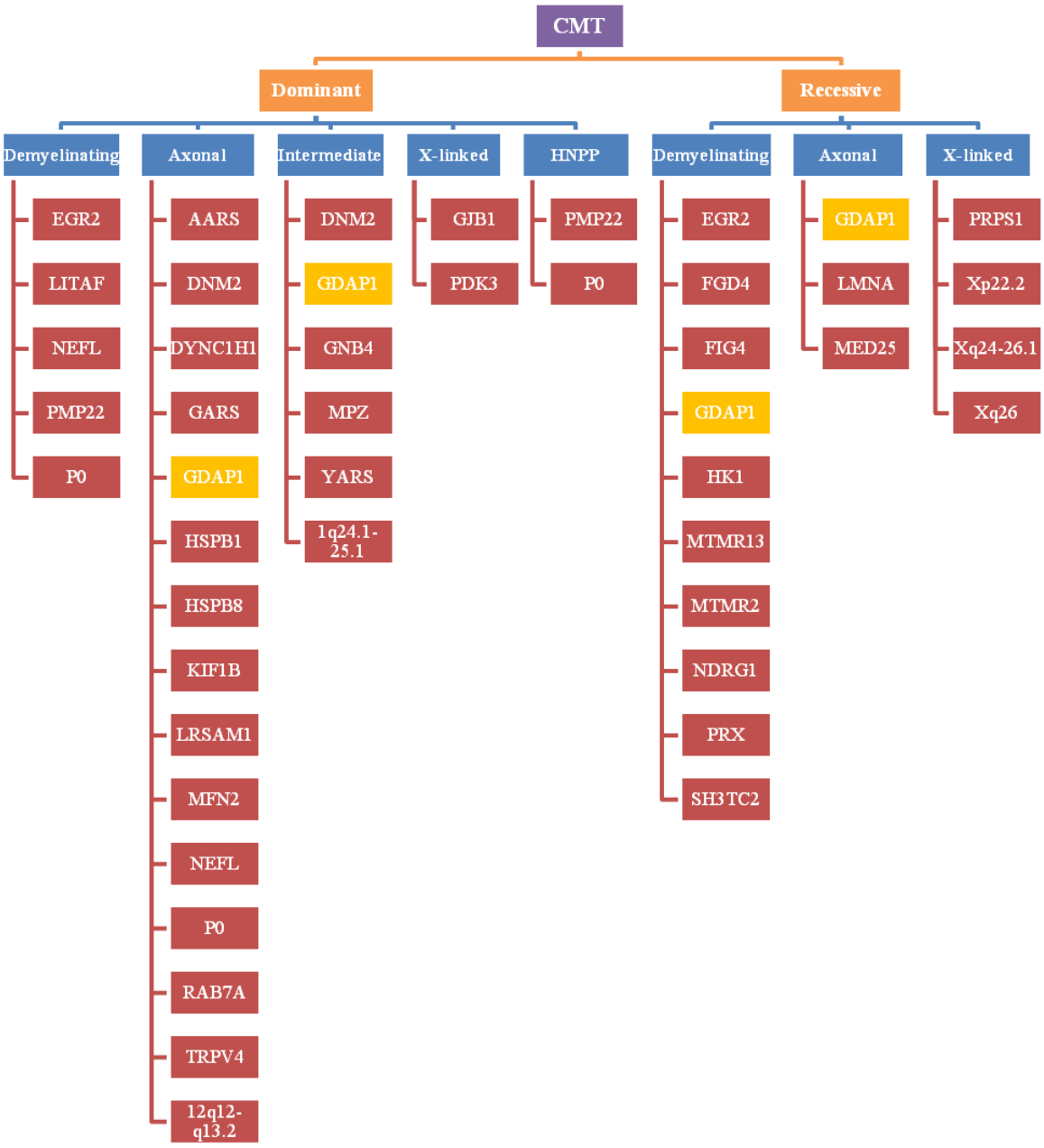

Figure 1.1. Genes and loci associated with Charcot-Marie-Tooth disease according to segregation and disease subtype (Siskind *et al*., 2013; Vallat *et al*., 2013).

The current research on CMT focuses not only on finding new causative genes, but also understanding the mechanisms that are important in the pathogenesis. Genes associated with CMT have diverse cellular functions and therefore understanding the pathogenesis for each gene (and sometimes different phenotypes caused by different mutations in the same gene) makes it necessary to develop *in vitro* and *in vivo* models (Figure 1.2).

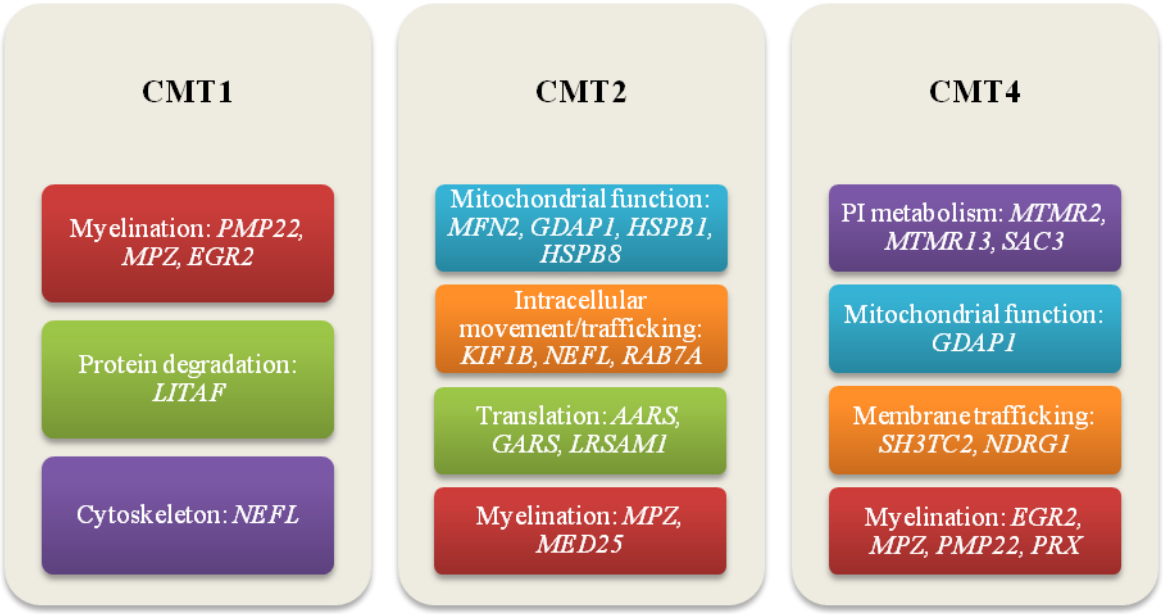

Figure 1.2. Major cellular and molecular mechanisms associated with CMT subtypes and related causative genes (Bucci, Bakke, & Progida, 2012; Zuchner & Vance, 2006).

To this date, functions of most of the CMT-associated genes have been studied using *in vitro* experiments. Recently, there have also been developments in modeling CMT for different causative genes using various model organisms. These include mouse models for the subtypes CMT1A (*PMP22*), CMT1B (*MPZ*), CMT1D (*EGR2*/*KROX-20*), CMT1E (*PMP22*), CMTX (*Cx32*/*GJB1*), CMT4B1 (*MTMR2*), CMT4B2 (*MTMR13*), CMT4F (*PRX*), fly model for DI-CMTC (*YARS*) and a zebrafish model for CMT2A (*MFN2*) (Chapman, Bennett, Ramesh, De Vos, & Grierson, 2013; Fledrich, Stassart, & Sereda, 2012; Storkebaum *et al*., 2009).

1.1. *GDAP1*

Among the most frequently mutated CMT causative genes, the *Ganglioside-induced Differentiation-Associated Protein 1* (*GDAP1*) gene is one of the least studied. Even though the knowledge on *GDAP1* is limited, this is one of the most promising CMT genes to study because the mutations in this gene cause distinct phenotypes including: mild to very severe disease progression with late and early onset, dominant and recessive segregation, and finally, demyelinating, axonal and intermediate forms (Cassereau *et al*.,

2011). Furthermore it is one of the most common CMT-causative genes with approximately 25% of autosomal recessive CMT cases (Senderek *et al*., 2003).

GDAP1 has six exons and two isoforms, isoform a (358 amino acids) and isoform b (290 amino acids), which are expressed ubiquitously, with higher expression in neurons as well as myelinating Schwann cells (Cuesta *et al*., 2002; Niemann, Ruegg, La Padula, Schenone, & Suter, 2005; Pedrola *et al*., 2008). The protein has two glutathione S-transferase domains (GST-N and GST-C), a hydrophobic domain (HD1) and a transmembrane domain (TM) as well as two predicted alpha helices that form the α4-α5 loop (Figure 1.3) (Marco, Cuesta, Pedrola, Palau, & Marin, 2004; Niemann, Wagner, Ruegg, & Suter, 2009). Besides the GST domains, which suggest a function in oxidative stress mechanisms, GDAP1 is shown to localize to the mitochondrial outer membrane and function as a mitochondrial fission factor (Niemann *et al*., 2005; Pedrola *et al*., 2005).

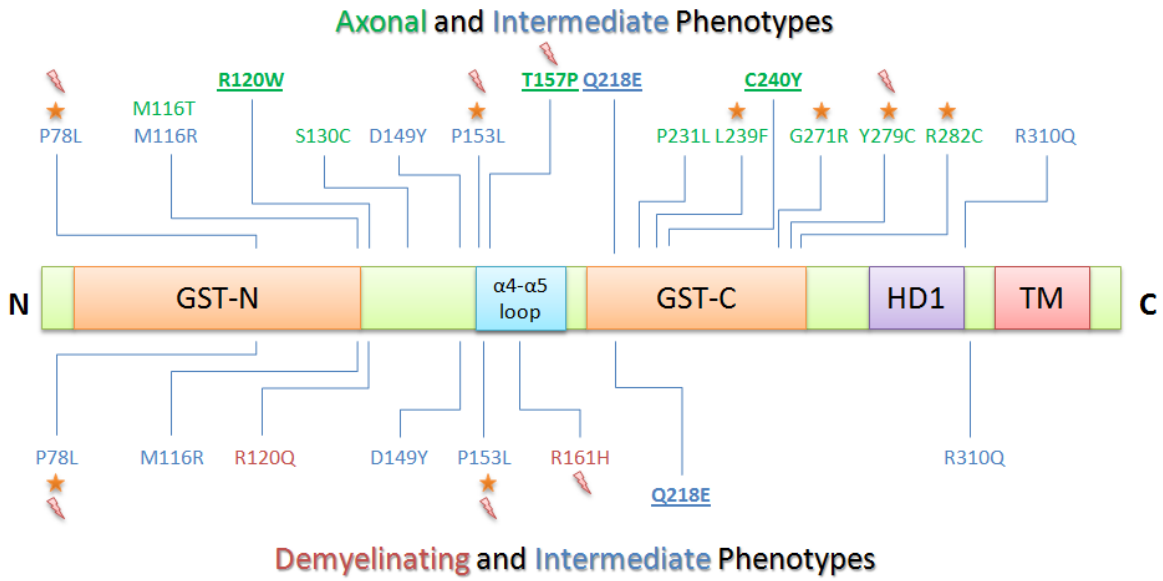

Figure 1.3. The domains and CMT-causing missense mutations of *GDAP1* according to disease phenotype. Underlined: dominant; Star symbol: conservation in *Drosophila melanogaster*; thunder symbol: severe phenotype (Cassereau *et al*., 2011).

Several mutations in *GDAP1* have been identified as CMT-causative and the majority of these are missense mutations (56%) along with frameshift (20%), nonsense (17%) and splicing (7%) mutations (Cassereau *et al*., 2011). Except for four dominant mutations, which have milder disease phenotypes in general, all of *GDAP1* mutations are

recessive and they mostly result in severe forms with early onset. The CMT subtypes caused by mutations in *GDAP1* are CMT2K (OMIM: 607831), CMT4A (OMIM: 214400), AR-CMT2 (OMIM: 607706), and CMTRIA (OMIM: 608340) (Baxter *et al*., 2002; Cuesta *et al*., 2002; Senderek *et al*., 2003; Sivera *et al*., 2010).

CMT2K is an axonal subtype and is caused by rare dominant mutations of *GDAP1*. Although more studies are necessary for validation in a larger cohort, it was shown that 27% of all CMT2 cases with dominant segregation were caused by *GDAP1* mutations (Crimella *et al*., 2010). The effect of CMT2K mutations are generally less severe and mostly later onset compared to other *GDAP1* mutations (Cassereau *et al*., 2011; Sivera *et al*., 2010).

CMT4 is the group of recessively segregating demyelinating and axonal neuropathies and its subtypes are listed according to the causative gene. The CMT4A subtype is caused by mutations in *GDAP1*. This subtype is a very severe form of CMT with early onset and progression of weakness towards upper limbs in the first decade, resulting in wheelchair dependence for some patients by their second decade (Boerkoel *et al*., 2003). The patients exhibit features of both demyelinating and axonal neuropathy with decreased touch sensation, loss of deep tendon reflex, undetectable or decreased mNCV due to distal atrophy, loss of large myelinated fibers, onion bulb formations, moderate or mild loss of smaller myelinated fibers and unmyelinated fibers, and lastly axonal atrophy (Boerkoel *et al*., 2003; Senderek *et al*., 2003; Sevilla *et al*., 2003). Other features associated with some of the CMT4A patients are vocal cord paralysis, hoarseness of the voice, facial weakness, all of which suggest central nervous system (CNS) involvement (Boerkoel *et al*., 2003).

Some of the *GDAP1* mutations that cause CMT4A phenotype are categorized as a new subtype AR-CMT2 due to the vocal cord paresis observed in the patients. Autosomal recessive axonal CMT with vocal cord paresis cases are similar to CMT4A in all aspects.

Rare *GDAP1* mutations also cause autosomal recessive intermediate subtype CMTRIA with limited sensory involvement, the only major difference from CMT4A (Senderek *et al*., 2003). The patients exhibit severe, early-onset neuropathy with intermediate mNCVs, with weakness starting at lower limbs and expanding proximally,

making the patients unable to walk without assistance in the second decade (Senderek *et al*., 2003).

1.1.1. Mitochondrial Dynamics

Mitochondrial dynamics is a continuous process that involves four organelle level events that allow mitochondria and thereby the cell to function properly: fusion and fission of mitochondria, mitophagy and mitochondrial motility (Chen & Chan, 2009). Balanced mitochondrial dynamics protect the integrity and homogeneity of mitochondria and mitochondrial DNA, sustain mitochondrial turnover and finally allow a functional electrical and biochemical subcellular environment for their proper function (Berman, Pineda, & Hardwick, 2008). Since energy production is necessary for survival of the cell, the perturbations of the mitochondrial dynamics affect cells that have high energy demand, like neurons. Therefore, many neurodegenerative diseases, including CMT, dominant optic atrophy, Parkinson's, Alzheimer's and Huntington's diseases, involve disruption of mitochondrial dynamics (Chen & Chan, 2009; Detmer & Chan, 2007).

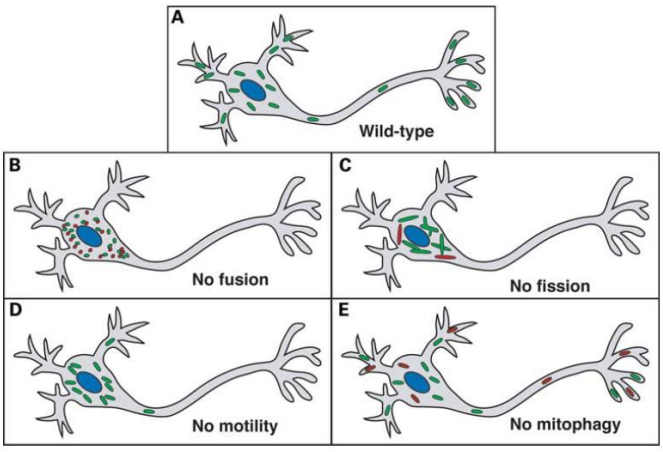

Figure 1.4. Mitochondrial dynamics defects in neurons (Chen & Chan, 2009).

Many of the proteins involved in mitochondrial dynamics have been identified and human proteins responsible for mitochondrial fusion are MFN1, MFN2 and OPA1, whereas those involved in fission are DRP1 and FIS1, which are all GTPases except for Fis1 (Chen & Chan, 2005). While MFN1 and MFN2 are located on the outer membrane of mitochondria, OPA1 is an intermembrane protein facing the inner membrane, as these

proteins are vital for fusion of outer and inner membrane of mitochondria, respectively (Chen & Chan, 2005). DRP1, which is a cytosolic protein, is responsible for fission of mitochondria when it localizes to the outer membrane and constricts the organelle in the presences of FIS1, which is also located on the outer membrane (Chen & Chan, 2005).

As GDAP1 is located on the mitochondrial outer membrane, much research has been put into its potential function in mitochondrial dynamics and pathogenic role in CMT. It was found that GDAP1 overexpression increased mitochondrial fragmentation, while its downregulation resulted in mitochondria of tubular structure (Niemann *et al*., 2005). It was also found that CMT-associated truncated forms of GDAP1 did not target mitochondria and therefore may have caused CMT by disrupting mitochondrial dynamics, similar to MFN1/MFN2 (Niemann *et al*., 2005). It was also observed that the majority of GDAP1 mutations, which are recessive, caused reduced activity contrary to the few dominant mutations, which were affecting fusion activity and neither of these mutation types caused their phenotype through apoptosis (Niemann *et al*., 2009). Although initial findings regarding increased reactive oxygen species production and disturbed mitochondrial membrane potential were only associated with dominant mutations of GDAP1, recently it was shown that recessively inherited GDAP1 mutant CMT patients had reduced glutathione concentration and mitochondrial membrane potential in their fibroblasts (Niemann *et al*., 2009; Noack *et al*., 2012).

1.1.2. Glutathione S-transferases

Glutathione S-transferases (GSTs) are enzymes that catalyze the conjugation reaction of glutathione (GSH) to electrophilic substrates, such as xenobiotics, reactive oxygen species (ROS) and other dangerous cellular byproducts (Eaton & Bammler, 1999). The GSTs are categorized into three major groups, depending on their cellular localization and cytosolic ones form the largest group (Figure 1.5). These groups are further categorized according to sequence similarity (Raza, 2011). GSTs are highly expressed in humans and constitute as high as 4% of all soluble protein's in liver. The soluble GSTs function as dimers (Eaton & Bammler, 1999). It is known that GSTs not only take part in detoxification, but in cell signaling and post-transcriptional modification pathways,

through interaction with kinases and S-glutathionylation (Laborde, 2010; McIlwain, Townsend, & Tew, 2006).

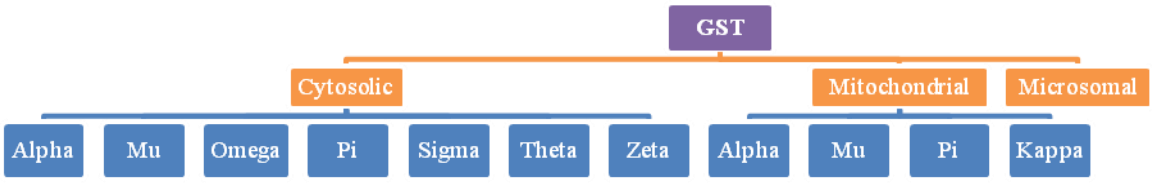

Figure 1.5. Categorization of GSTs according to their localization (Raza, 2011).

Since *GDAP1* was shown to have two GST domains, it was thought to be involved in oxidative stress mechanisms (Marco *et al*., 2004). Although initial *in vitro* studies revealed no functional GST activity for GDAP1, these findings may not be representative of GDAP1's function in the cell as the protein used in the experiment lacked a transmembrane domain since the full-length protein formed dimers and remained insoluble (Pedrola *et al*., 2005; Shield, Murray, & Board, 2006). Recently, it was shown that GDAP1 overexpression in neuronal cells resulted in reduction of oxidative stress and protection of mitochondrial integrity whereas its knockdown resulted in sensitivity to oxidative stress (Noack *et al*., 2012). It was also shown that CMT-causing recessive mutant forms of GDAP1 did not have such positive effects on lowering oxidative stress, indicating that GDAP1 does indeed possess GST activity (Noack *et al*., 2012).

Though GDAP1 is not a cytosolic protein, it most closely resembles the cytosolic class of GSTs, especially Zeta, Omega and Theta subclasses at the sequence level (Marco *et al*., 2004). However, bioinformatics analyses have also shown that GDAP1 is a distinct GST and has three major features separating it from canonical GSTs (Marco *et al*., 2004). GDAP1 and its paralog GDAP1L1 belong to a novel class of GST-like proteins (GDAP1 class) as the two have a transmembrane and hydrophobic domain unlike most other GSTs, which are cytosolic, have low sequence similarity with other GSTs and finally have an extra loop of alpha helices, which is absent in other GSTs (Marco *et al*., 2004). As GSH is produced in the cytosol and then transported to mitochondria, which results in an internal mitochondrial pool of GSH to be coupled to ROS by mitochondrial GSTs. Oxidative stress in the mitochondrial internal environment of mitochondria is maintained separately; thus

GDAP1, being located on the outer membrane of mitochondria may have a role in this process (Raza, 2011; Sun *et al*., 2012).

1.2. *Drosophila melanogaster*

Drosophila melanogaster, an insect that belongs to the order *Diptera*, is one of the most widely used model organisms. Cultured at 25°C, it takes 10 days for a fertilized egg to become a fertile adult. The life span of well-kept *Drosophila* is approximately 60 days for females (shorter for males) and this can be extended by lowering the temperature and using different fly food. The fertilized egg goes through four stages: embryo (1 day), larva (4 days, formed of first, second and third instar stages), pupa (4 days) and adult. During pupariation, the organism goes through metamorphosis and 10 pairs of imaginal discs that grew during larval stages form completely new structures such as eye, wing, antenna and leg. For instance, during this metamorphosis, neurons innervating larval muscles retract and form new connections to adult musculature. Therefore, any process analyzed in flies should be carefully studied in larval, pupal and adult stages, if possible (Lloyd & Taylor, 2010).

Drosophila as a model organism has been widely used for the last few decades in laboratories, not only due to its short life cycle, low cost and ease of handling, but also for its highly developed genetic toolkit that includes tools such as drivers (GAL4 lines) and balancers (multiply inverted chromosomes) for overexpressing a gene spatiotemporally and keeping an allele in a heterozygous state, respectively. Furthermore, fundamental aspects of cell biology are similar across species, which allows comparative analysis of a molecular process essential for humans. Considering that approximately 77% of all genes that are known to be causative for a human disease have homologs in *Drosophila*, the fly becomes a perfect organism to model diseases (Reiter, Potocki, Chien, Gribskov, & Bier, 2001). Among flies and mammals, the amino acid identity between two homolog genes is approximately 40%, though this value increases to near 90% for some of the conserved domains (Pandey & Nichols, 2011). With *Drosophila*, it is possible to score phenotypes in an unbiased way, use well-established behavioral assays and easily conduct drug screens.

There are two major advantages of using flies to develop a disease model compared to mammalian models: the ease of doing a drug screen and the ability to find modifier genes by overexpressing or downregulating a library of genes together with the target disease gene to find an interaction. Development of a *Drosophila* model is especially favorable for genetically heterogeneous diseases since in this case many mutations in different genes may be associated with the disease and it is impractical to develop rodent models to analyze each mutation, whereas it is relatively easy in flies.

As the fly has many advantages for studying human diseases, *Drosophila* models have been generated for many diseases, including motor neuron disorders (spinobulbar muscular atrophy, spinal muscular atrophy, amyotrophic lateral sclerosis), myopathies (Duchenne muscular dystrophy, myotonic dystrophy) and neurological disorders (Huntington's, Alzheimer's diseases and Fragile-X syndrome) (Lloyd & Taylor, 2010). According to the Homophila database, 79% of CMT-associated genes have an ortholog in *Drosophila* and the average similarity between the two homologs is 63% while identity is 45% (Lloyd & Taylor, 2010). However, up to date, only a single fly model has been developed for Charcot-Marie-Tooth disease, which was for dominant mutations of tyrosyl-tRNA synthetase gene (*YARS*) (Storkebaum *et al*., 2009).

1.2.1. GAL4-UAS Binary System

Besides balancers, the most powerful tool in *Drosophila* genetics is the spatio-temporal control of expression via the GAL4-UAS system, which is adapted from the yeast. GAL4 is a yeast transcription factor, which binds to a short element called Upstream Activating Sequence (UAS) and results in transcriptional activation of the downstream gene. As expression of GAL4 in *Drosophila* resulted in no harmful effects for the organism, the system was adapted for use in flies (Duffy, 2002).

GAL4-UAS system is formed of two parts: a GAL4 driver line and a UAS responder line, which allow overexpression when found in the same genotype (Figure 1.6). A driver is a GAL4 gene cloned downstream of a promoter and/or enhancer that is found in the organism endogenously as the main regulatory element(s) for expression of a specific gene. These flies express GAL4 spatio-temporally according to the regulatory element

found in this driver (Figure 1.6a). The UAS responder line is a fly that has the coding sequence of a target to be expressed, such as Green Fluorescent Protein (GFP), Red Fluorescent Protein (RFP) or any gene of interest, in the downstream of a UAS element. In UAS responder lines, no expression of the target gene takes place as GAL4, which is necessary for transcriptional activation of the target gene, is not endogenously expressed in flies (Figure 1.6c). When a GAL4 driver line is crossed with a UAS responder line, a specific pattern of expression is obtained in the progeny that have both GAL4 and UAS in their genotype (Figure 1.6b).

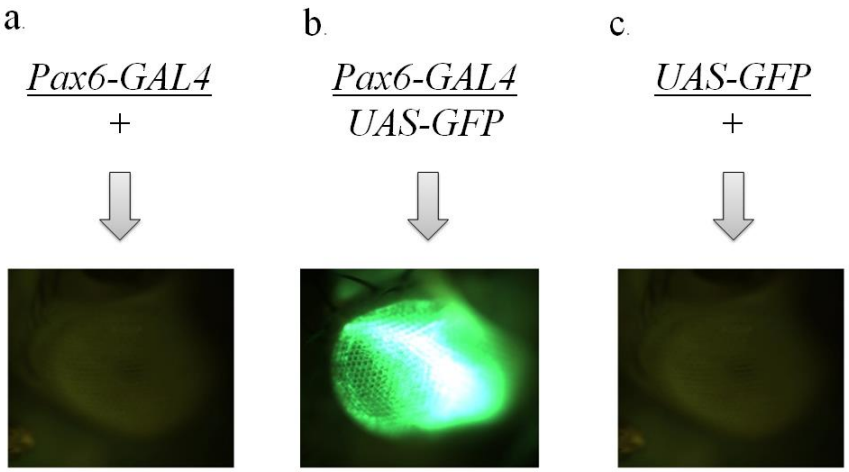

Figure 1.6. GAL4-UAS binary system in *Drosophila*. Pax6 is a transcription factor expressed in the eye. *Drosophila* eye for (a) Pax6-GAL4, (b) Pax6-GAL4 and UAS-GFP and (c) UAS-GFP lines, all exposed with GFP filter.

Expression patterns of drivers range from organism-wide to only a few cells and many of the drivers are commercially available such as act5c-GAL4 for ubiquitous expression, elav-GAL4 for panneuronal expression, OK6-GAL4 for expression in motor neurons and D42-GAL4 for expression in indirect flight muscle motor neurons. Besides allowing spatial expression, drivers that allow expression at different developmental stages are also available. It is also possible to find a stronger driver with the same expression pattern that causes even higher level of expression. It is also possible to use GAL80, the inhibitor of GAL4, in order to limit transcriptional activation at certain developmental stages using a heat shock promoter in the upstream of GAL80. This way, it is possible to overexpress a certain gene in larval stages and inhibit its expression using increased temperature in adulthood.

The use of the GAL4-UAS system, not only allows overexpression of a gene, but also its downregulation and RNAi libraries are commercially available for knockdown. A UAS-responder line that harbors a miRNA targeting the gene of interest is used in downregulation of the target gene spatiotemporally. Similarly, these lines can also be used to find modifier genes by crossing a certain mutant phenotype to an RNAi library searching for partial or full rescue of the phenotype in the progeny.

1.2.2. *P*-elements

The fly genome is formed of a pair of sex chromosomes and three autosomes (Figure 1.7). The X chromosome, left and right arms of second (2L and 2R) and third chromosomes (3L and 3R) are approximately equal in size while the fourth chromosome is smaller. Traditionally, radiation and chemicals such as ethylmethanesulfate were used to carry out random mutagenesis including point mutations and chromosomal aberrations and flies were isolated according to their mutant phenotypes. However, recently insertional mutagenesis using transposable elements have started to be utilized more and more as the advantages of this system are numerous. *P*-elements are the most commonly used transposons and they randomly integrate into the genome, allowing the addition of any sequences of certain length to the fly genome. The *P*-element vectors generally include a marker gene, mostly w^{+}, which causes red eye in flies allowing easy selection of transformants. Random integration using *P*-elements allow finding enhancers using enhancer trap screens, performing insertion mutagenesis to disrupt genes, or generating lines that overexpress a certain gene by including it in the targeting construct.

Figure 1.7. Chromosome setup of a male *Drosophila melanogaster*. The values over the chromosome arms are the range of segments that are used to define the location of a gene (Greenspan, 2004).

The *P*-element vectors that include short sequences called *attB*, bacterial attachment sites, allow site specific integration into fly genome. The prepared *P*-element construct is injected into flies that have similar short sequences called *attP*, phage attachment sites. In the presence of a recombinase (such as *ΦC31* recombinase) recombination between *attP* and *attB* sequences takes place, thus resulting in integration into the region where *attP* is located. The integration is irreversible as when *attB* and *attP* sites join, they change to *attL* and *attR*, which are not targets of the recombinase any more. Most commonly used *P*-elements include *pUAST* (random integration) and *pUASTattB* (site specific integration using *ΦC31* recombinase), which are overexpression vectors that allow cloning of any coding sequence downstream of a UAS element.

1.2.3. *Minos* Elements

As *P*-elements have been used for random integration into the genome for disrupting genes, it was found that these transposons integrate into hot spots, leaving certain regions uninterrupted (Metaxakis, Oehler, Klinakis, & Savakis, 2005). Therefore different types of transposable elements were analyzed to find ones that target randomly or in a different pattern than the *P*-elements to disrupt the whole *Drosophila* genome as a method to identify new genes. *Minos* elements from the *Tc1/mariner* family of transposons discovered in *Drosophila hydei* were found to be integrating relatively randomly with a bias towards regions that harbored TA dinucleotides, which are found in the intronic regions of many genes (Metaxakis *et al*., 2005). Since these transposons integrate into introns, they do not cause a phenotype in most cases. However, as with many other transposable elements, mobilization of a *Minos* element using its transposase could result in deletion of flanking sequences or insertion thereof at another location (Metaxakis *et al*., 2005).

1.2.4. Integrase-Mediated Approach For Gene Knock-Out

Classical ends-out homologous recombination system allows exchange of a sequence of interest using two flanking homology arms, a rare restriction enzyme recognition site (*I-Sce*I) and flippase recognition site (*FRT*), which work together to cut out and linearize a construct that is already integrated into the genome. With a linear DNA fragment that has

homologous regions to a chromosome, the endogenous mechanism may allow a rare event of homologous recombination to take place between the homology arms and the target locus. Recently, classical ends-out homologous recombination was improved with the addition of *attP* sites to the classical ends-out homologous recombination vector, creating the *pPwhite-STAR* targeting vector: integrase-mediated approach for gene knock-out (IMAGO) (Choi *et al*., 2009).

In the IMAGO system (Figure 1.8), after the targeting vector is integrated into the genome at a pre-selected site (Figure 1.8a), heat-shock is used to activate the rare restriction enzyme *I-Sce*I and flippase resulting in mobilization of a fragment that includes the marker gene such as w^+ flanked by homology arms that are suitable for the target gene's flanking region, and finally *attP* sites at the very ends (Figure 1.8b and 1.8c) (Figure 1.8d).

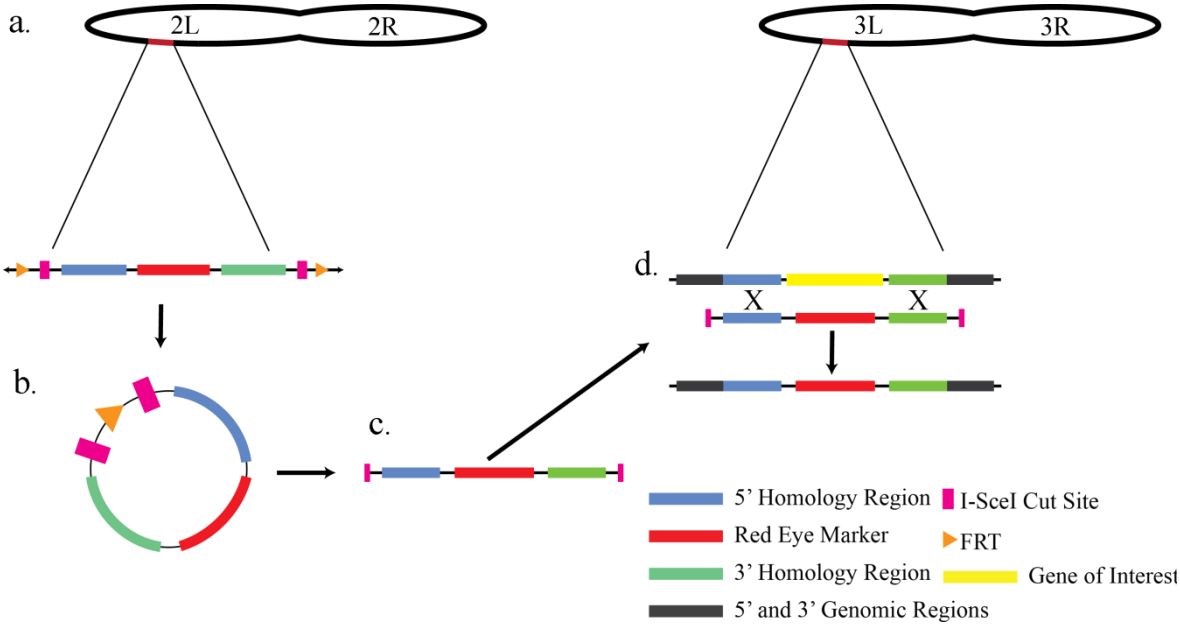

Figure 1.8. Ends-out homologous recombination using IMAGO. (a) Integration of the targeting construct into genome, (b) flipping out of the construct by flippase activity, (c) linearization of the flipped out circular DNA by *I-Sce*I, (d) alignment of the targeting linearize targeting construct to its endogenous region and homologous recombination.

The *attP* sites are used later on as landing sites for recombinase mediated cassette exchange (RMCE) (Figure 1.9). In other words, once the IMAGO construct is mobilized

and the target gene is replaced with the marker gene, *attP* sites flanking this marker gene can then be used to replace the marker with any sequence of interest. In this way, it is possible to knock-in the homolog of the knocked-out gene as a rescue experiment, mutant forms of the gene to analyze an expected phenotype or a reporter/tagged version to study its expression pattern.

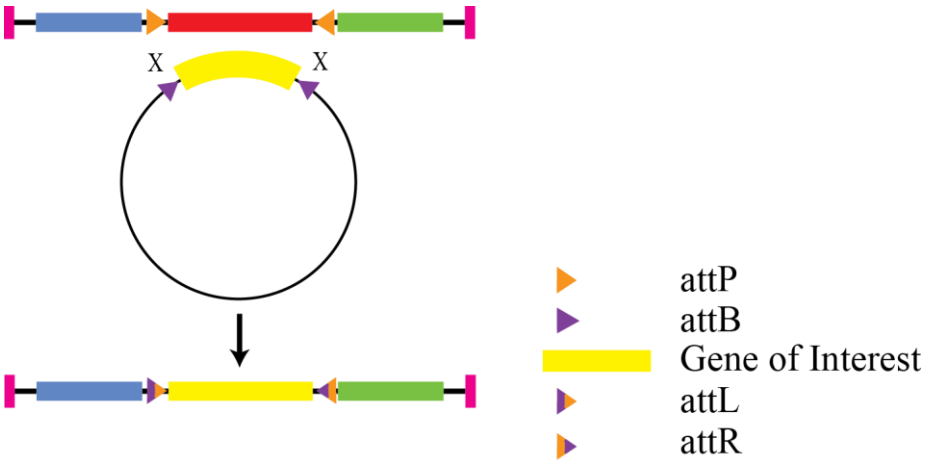

Figure 1.9. Knocking-in a gene of interest using recombinase mediated cassette exchange.

1.3. *CG4623*

According to the NCBI's protein blast tool (BLASTP 2.2.28+), *CG4623* is the homolog of *GDAP1* in *Drosophila melanogaster* with 29% amino acid identity (98 residues identical out of 343) and 46% amino acid similarity (161 residues positive out of 343) (Altschul *et al*., 1997; Altschul *et al*., 2005). Previous bioinformatics analyses have shown that *CG4623* bears close similarity to *GDAP1* and *GDAP1L1* compared to its resemblance of all other GSTs (Marco *et al*., 2004). Among *Drosophila* GSTs, *CG4623* was found to be a quick-evolving gene (Low *et al*., 2007). However, there isn't much information about the function of CG4623 in the literature.

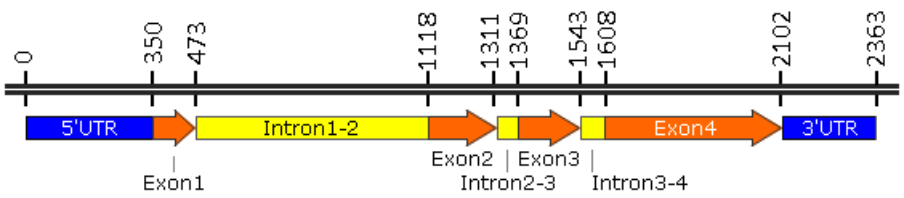

Figure 1.10. *CG4623* gene showing its length and gene structure.

CG4623 is located on the left arm of the third chromosome (3L) on position 64C7 and spans a length of approximately 2.3 kb with four exons (Figure 1.10). The major polypeptide coded by this gene (Isoform A) is 37.6 kD in weight and is formed of 327 amino acids. According to the ModENCODE database, *CG4623* is spatially expressed at very low levels in imaginal discs, salivary glands, head and carcass, at low levels in the testis, larva and adult digestive system, and at moderate levels in accessory gland and adult digestive system (Cherbas *et al*., 2011). Temporally, *CG4623* is expressed throughout the organism's lifespan with highest expression in embryonic and larval stages and higher expression is found in the adult males compared to the females (Graveley *et al*., 2011).

2. AIM OF THE STUDY

In this study, our aim is to develop a *Drosophila* model for Charcot-Marie-Tooth disease, specifically for its subtypes caused by *GDAP1* mutations.

In order to develop the disease model, we aim to knock-in wildtype and mutant *GDAP1* in place of the fly homolog, *CG4623*. Based on integrase-mediated approach for gene knock-out (IMAGO), constructs for knocking-in wildtype *GDAP1*, nine mutant forms of *GDAP1*, a *CG4623-GAL4* driver and an mCherry reporter for *CG4623* were generated.

In the second part, in order to assess the effect of *CG4623* overexpression *in vivo* and compare it to the findings regarding *GDAP1* overexpression, a UAS-*CG4623* line was generated.

Last aim of the project was to test techniques of longevity and mitochondrial dynamic analysis on available mutants of mitochondrial dynamics related genes, for adaption of these techniques to analyze the generated lines in the future.

3. MATERIALS

3.1. Biological Materials

In this study the fly lines listed in Table 3.1 have been used, which were commercially available, except for the UAS-CG4623 line, which was generated by the author. All of these flies were kept in incubators with 12 hour light and 12 hour dark cycles at 25°C with a humidity of 80%. Fly food was prepared according to manufacturer's instructions using Nutri-Fly Bloomington Formulation; it was changed every three weeks for stocks and in shorter periods for other fly lines and crosses.

Table 3.1. Fly lines used in this research.

Genotype	**Chromosome**	**Description**
w^{1118}	I	White eye
Df(1)Exel6239	I	Deletion of a chromosomal region including *Marf*
FM7a	I	Balancer chromosome
FM7c	I	Balancer chromosome
y, v	I	Yellow body color, vermillion eye
y, w	I	Yellow body color, white eye
Act5C-GAL4	II	Ubiquitous driver
CyO	II	Balancer chromosome with curly wings
CyO, Roi	II	Balancer chromosome with rough eye
Df(2L)Exel6008	II	Deletion of a chromosomal region including *Drp1*
$Drp1^{T26}$	II	Mutant allele of *Drp1*
Sco	II	Scutoid marker
sp	II	Supernumerary bristles marker
UAS-mitoGFP	II	Overexpresses GFP with mitochondrial import signal
D42-GAL4	III	Motor neuron driver
TM2	III	Balancer chromosome with large halteres

Table 3.1. Fly lines used in this research. (cont.)

TM3, sb	III	Balancer chromosome with shorter bristles
TM6B, hu, tb	III	Balancer chromosome with humoral and tubby markers
UAS-CG4623	III	Overexpresses *CG4623*
UAS-Drp1-RNAi	III	Overexpresses dsRNA targeting *Drp1*
UAS-Marf-RNAi	III	Overexpresses dsRNA targeting *Marf*

3.2. Chemicals and Enzymes

In this study the following list of chemicals and enzymes were used (Table 3.2). All of the DNA markers used were supplied by Thermo Scientific, USA: 1kB (#SM0311), denoted in the text as "marker", 100 bp (#SM0242), denoted in the text as "marker s" and Lambda DNA/HindIII (#SM0103), denoted in the text as "marker l".

Table 3.2. List of chemicals and enzymes.

Chemical	**Supplier and product code**
Agarose	Prona Agarose, Biomax, EU (124543PR)
Ampicillin	Mustafa Nevzat, Turkey (Ampisina)
Bovine serum albumin	Sigma-Aldrich, USA (A2153)
Chloramphenicol	Applichem, Germany(7495)
*Dpn*I	New England Biolabs, USA (R0176S)
EDTA	Sigma-Aldrich, USA (34549)
Ethidium bromide solution	Sigma Life Sciences, USA (E1510)
FastDigest *BamH*I	Thermo Scientific, USA (FD0054)
FastDigest *Eco*RI	Thermo Scientific, USA (FD0275)
FastDigest *Eco*RV	Thermo Scientific, USA (FD0303)
FastDigest *Hind*III	Thermo Scientific, USA (FD0504)
FastDigest *Kpn*I	Thermo Scientific, USA (FD0524)
FastDigest *Nhe*I	Thermo Scientific, USA (FD0973)
FastDigest *Sac*I	Thermo Scientific, USA (FD1133)
FastDigest *Sma*I	Thermo Scientific, USA (FD0663)

Table 3.2. List of chemicals and enzymes. (cont.)

FastDigest *Xba*I	Thermo Scientific, USA (FD0684)
FastDigest *Xho*I	Thermo Scientific, USA (FD0694)
Formaldehyde	Sigma-Aldrich, USA (47608)
HEPES	Sigma-Aldrich, USA (H4034)
Kanamycin	Life Technologies, USA (11815-024)
KCl	Merck, Germany (TA741635)
LB agar	Difco, France (244520)
LB broth	Difco, France, (244620)
Magnesium chloride hexahydrate	Carlo Erba Reagenti, Italy (7791186)
Normal goat serum (NGS)	Millipore, Germany (S26-100ML)
PfuUltra HF DNA polymerase	Agilent Technologies, USA (600385)
pGEM-T Easy vector system I	Promega, USA (A1360)
Phosphate buffered saline (10X)	Life Technologies, USA (70011-044)
Phusion HF DNA polymerase	New England Biolabs, USA (M0530S)
Potassium chloride	Sigma-Aldrich, USA (P9541)
Silicone elastomere kit	Fisher Scientific, UK (NC9644388)
Sodium acetate	Merck, Germany (1.06265)
Sodium bicarbonate	Sigma-Aldrich, USA (S7277)
Sodium chloride	Sigma-Aldrich, USA (S7653)
Sodium deoxycholate	Sigma-Aldrich, USA (30970)
Sucrose	Sigma-Aldrich, USA (S0389)
Taq DNA polymerase (recombinant)	Thermo Scientific, USA (EP0405)
Trehalose	Sigma-Aldrich, USA (T9531)
Tris	Sigma-Aldrich, USA, (T1503)
Triton X-100	Sigma-Aldrich, USA (T8787)
T4 DNA ligase	Thermo Scientific, USA (EL0014)
VectaShield mounting medium	Vector Laboratories, USA (H-1000)

3.3. Buffers and Solutions

The buffers and solutions are listed in Table 3.3 with their contents.

Table 3.3. List of buffers and solutions used in the study.

Buffer or solution	**Content**
1% agarose gel	1X TAE buffer 1% agarose 0.5% ethidium bromide
1X TAE buffer	40 mM Tris-HCl 1 mM EDTA 0.1% acetic acid
Blocking Solution for NMS dissection	10% NGS in PBX4
Ethidium bromide solution	10 mg/ml in dH_2O
Fixation Solution for NMS dissection	3.7% formaldehyde Solution in HL3
HL-3 Solution	110 mM NaCl 5 mM KCl 10 mM $NaHCO_3$ 5 mM HEPES 30 mM sucrose 5 mM trehalose 10 mM $MgCl_2$ (pH=7.2)
PAX DG	10 g BSA 3 g sodiumdeoxycholate 3 ml Triton X-100 50 ml NGS 100 ml PBS (10X) dH_2O to a total of 1 liter
PBS (1X)	100 ml PBS (10X) 900 ml dH_2O
PBX3	0.3% Triton X-100 PBS (1X) to a total of 1 liter
PBX4	0.4% Triton X-100 In PBS (1X)

All of the other buffers and solutions are purchased ready-made (such as 10X PBS) or prepared according to the manufacturers' instructions (such as LB broth).

3.4. Oligonucleotide Primers and cDNAs

In this study the following lists of chemicals were synthesized at Macrogen company (South Korea). The lyophilized primers were suspended in suitable amount of dH_2O to reach a concentration of 100 mM. Primers used for cloning and sequencing can be found in Table 3.4.

Table 3.4. List of primers used for cloning and sequencing.

Primer Name	**Primer Sequence (5'→3')**	**T_m (°C)**
T7_FP	TAATACGACTCACTATAGGG	48
SP6_RP	ATTTAGGTGACACTATAGAAT	47
CG4623_pUAST_FP	CTCGAGATGAGCGAGCAGACAAAGG	63
CG4623_pUAST_RP	TCTAGAGCTCACTTGTGCGCGAAGG	64
pUAST_seq_FP	CCAGCAACCAAGTAAATCAACTGC	59
pUAST_seq_RP	ATCTCTGTAGGTAGTTTGTCC	52
Gal4_pABC_FP	TACAAGCTTATGAAGCTACTGTCTTCTATCG	60
Gal4_pABC_RP	ATAGGTACCTTACTCTTTTTTTGGGTTTGGTGG	62
mCherry_pABC_FP	TACAAGCTTATGGTGAGCAAGGGCGAGGAG	67
mCherry_pABC_RP	ATAGGTACCTACTTGTACAGCTCGTCCATGC	64
pABC_seq_FP	GCGGGCCTCTTCGCTATTAC	59
pABC_seq_RP	CACTTTATGCTTCCGGCTCG	57
CG4623_Upstream_FP	TTCAGCGGTTTGCCATTCAC	58
CG4623_Downstream_RP	GAGAGCAGCCATCAAGCATAG	57
CG4623_pET30a_FP	GGTACCAAGATGAGCGAGCAGACAAAGG	64
CG4623_pET30a_RP	CTCGAGCTCACTTGTGCGCGAAGG	65
GAL4_Int_Seq1_FP	CCACAACATCCCGTTTACTTC	55
GAL4_Int_Seq2_FP	CACCCTTGGCTATCCTTTAC	54
GDAP1_pABC_FP	AAGCTTATGGCTGAGAGGCAGGAAG	62
GDAP1_pABC_RP	GGATCCTAGAAATAATTTGGTCTGGGTCTAAATGC	62

For site-directed mutagenesis reactions, the primers listed in Table 3.5 were used.

Table 3.5. List of primers used in site-directed mutagenesis.

Primer Name	**Primer Sequence (5'→3')**	**T_m (°C)**
GDAP1_pABC_FP	AAGCTTATGGCTGAGAGGCAGGAAG	62
GDAP1_pABC_RP	GGATCCTAGAAATAATTTGGTCTGGGTCTAAATGC	62
GDAP1_P78L_FP	TCAACTGGAGAAGTGCTTGTCCTTATCCACGGG	68
GDAP1_P78L_RP	CCCGTGGATAAGGACAAGCACTTCTCCAGTTGA	68
GDAP1_R120Q_FP	CCTGATAAAGAAAGCATGTATTACCCACAGGTACAACATTACC	66
GDAP1_R120Q_RP	GGTAATGTTGTACCTGTGGGTAATACATGCTTTCTTTATCAGG	66
GDAP1_R120W_FP	CCTGATAAAGAAAGCATGTATTACCCATGGGTACAACATTACC	66
GDAP1_R120W_RP	GGTAATGTTGTACCCATGGGTAATACATGCTTTCTTTATCAGG	66
GDAP1_D149Y_FP	TCCTGAGTTAACTGTGTACTCCATGATCCCGGC	67
GDAP1_D149Y_RP	GCCGGGATCATGGAGTACACAGTTAACTCAGGA	67
GDAP1_P153L_FP	TGTGGACTCCATGATCCTGGCTTATGCAACTACAA	67
GDAP1_P153L_RP	TTGTAGTTGCATAAGCCAGGATCATGGAGTCCAC A	67
GDAP1_T157P_FP	TGATCCCGGCTTATGCACCTACAAGGATTCGTAGC	69
GDAP1_T157P_RP	GCTACGAATCCTTGTAGGTGCATAAGCCGGGATCA	69
GDAP1_C240Y_FP	GGCCAGCAACCTTGGCTCTACGGTGAATCC	69
GDAP1_C240Y_RP	GGATTCACCGTAGAGCCAAGGTTGCTGGCC	69
GDAP1_G271R_FP	GGAGAAACTGGGGAAACAGAAAGCGACCAAACTTG	67

Table 3.5. List of primers used in site-directed mutagenesis. (cont.)

GDAP1_G271R_RP	CAAGTTTGGTCGCTTTCTGTTTCCCCAGTTTCTCC	67
GDAP1_Y279C_FP	GACCAAACTTGGAAACCTGTTACGAGCGTGTCTTGAA	68
GDAP1_Y279C_RP	TTCAAGACACGCTCGTAACAGGTTTCCAAGTTTGGTC	68

GDAP1 cDNA for transcript variant 1 from Origene, USA (SC317569) and CG4623 cDNA from Drosophila Genomics Resource Center, USA (RE69232) were used in this study.

3.5. Antibodies

The following list of antibodies have been used in the immunohistochemistry (Table 3.6).

Table 3.6. Antibodies used in immunohistochemistry.

Antibody	**Antigen**	**Host**	**Dilution**	**Producer**
Anti-elav	Elav/neuron	Rat	1:50	DSHB
Anti-repo	Repo/glia	Mouse	1:20	DSHB
Anti-DCSP-2	Cysteine-string protein	Mouse	1:100	DSHB
Anti-GFP	GFP	Rabbit	1:500	Torrey Pines Biolabs
Alexa 488	Rabbit	Goat	1:1000	Invitrogen
Alexa 555	Mouse	Goat	1:1000	Invitrogen
Alexa 633	Rat	Goat	1:1000	Invitrogen

3.6. Disposable Materials

The following table lists the disposable materials that have been used in this study (Table 3.7).

Table 3.7. List of disposable materials.

Material	**Producer**
Centrifuge tubes, 15 ml	Becton, Dickinson and Company, USA
Centrifuge tubes, 50 ml	Becton, Dickinson and Company, USA
Culture tubes, 14 ml	Greiner Bio-One, Belgium
Petri dishes (60 mm)	Isolab, Germany
Petri dishes (90 mm)	Isolab, Germany
Filtered tips	Fisher Scientific, UK
Pipette tips	Fisher Scientific, UK
Microscope cover glass	Isolab, Germany
Positively charged slides	Thermo Scientific, USA
Pasteur pipettes	Isolab, Germany
Microcentrifuge tubes, 0.5 ml	Fisher Scientific, UK
Microcentrifuge tubes, 1.5 ml	Fisher Scientific, UK
Microcentrifuge tubes, 2 ml	Fisher Scientific, UK
Microseal PCR sealers	Bio-Rad, USA
PCR tubes (200 µl)	Fisher Scientific, UK
PCR strips (8 well)	Fisher Scientific, UK
PCR plates (96 well)	Fisher Scientific, UK

3.7. Laboratory Equipment

The following table lists the laboratory equipment used throughout this project (Table 3.8).

Table 3.8. List of laboratory equipment.

Equipment	**Producer**
Autoclave	Astell Scientific Ltd., UK
Centrifuges	Centrifuge 5415 (Eppendorf, Germany)
Cold room	Birikim Elektrik Soğutma, Turkey
Confocal microscopy system	TCS SP5 (Leica Microsystems, USA)
Dissection forceps	FST, USA
Dissection scissors	WPI, USA

Table 3.8. List of laboratory equipment. (cont.)

Electrophoresis equipment	Mini-Sub Cell (Bio-Rad, USA)
Fluorescence stereomicroscope	MZ16FA (Leica Microsystems, USA)
Freezers	20 ºC (Bosch, Germany)
Gel documentation system	Bio-Rad Labs, USA (Gel Doc XR)
Magnetic stirrer	Speed Safe (Hanna Instruments, USA) MK 418 (Nüve, Turkey)
Fly incubators	TK 120 (Nüve, Turkey) TK 600 (Nüve, Turkey)
Laboratory bottles	Isolab, Germany
Micropipettes	Gilson, USA
Microwave oven	Arçelik, Turkey
Refrigerators	+4º C Arçelik, Turkey
Shaker	SL 350 (Nüve, Turkey)
Stereo microscope	Olympus, USA (SZ61)
Thermal cycler	Bio-Rad Labs, USA (C1000 Thermal Cycler)
Vortex mixer	Nuvemix (Nüve, Turkey)
Water bath	BM 302 (Nüve, Yurkey)

4. METHODS

4.1. Histological Methods

4.1.1. Dissection of Larval Brain and Ventral Nerve Cord

Third instar larvae were collected from vials and put in ice-cold 1X PBS. On silicone plates, a drop of 1X PBS was placed using a Pasteur pipette. A larva was taken from the solution with a forceps to a clean drop on the plate. Holding from the middle of the larva with one forceps, the mouth hook was pulled with another forceps until the brain and ventral nerve cord (VNC) was taken out. The remaining body was disposed of. The brain and the VNC were cleaned from any remaining cuticles, fat bodies and all imaginal discs except for antennal and eye discs. The dissected brains and VNJs were collected in 1X PBS on ice.

4.1.2. Immunohistochemistry of Larval Brain and Ventral Nerve Cord

After fixation of the collected organs in 4% paraformaldehyde in 1X PBS for 20 minutes, fixation solution was washed with PBX3 three times for 10 min each. Dissected organs were blocked with 200 µl of PAXDG for two hours. Blocking solution was replaced with new PAXDG solution containing proper primary antibodies and the collected organs were incubated on a shaker at 4°C overnight.

The next morning, primary antibody containing PAXDG was removed and the organs were washed three times for 10 min with 200 µl of PBX3. The samples were incubated in 200 µl of PAXDG solution after adding proper amounts of secondary antibodies for two hours at room temperature without shaking. After incubation with secondary antibody for 2 hours at room temperature, the samples were washed with PBX3 three times for 10 min. Then the samples were cleaned of any remaining trachaea and placed on a drop of mounting medium on microscopy slide with the same orientation. After organizing the organs, a cover slip was placed on top and all four sides were sealed with nail polish. Prepared slides were kept at 4°C. For visualization, Leica confocal

microscope with LAS AF software was used. The images obtained were processed and analyzed using ImageJ software.

4.1.3. Dissection of Larval Neuromuscular System

Third instar larvae were collected from vials and kept in fresh HL-3 solution while they were being dissected on silicone plates. A larva was pinned down from the anterior and posterior ends stretching longitudinally enough not to tear the larva. A hole at a central point in the body was poked using a pair of dissection scissors, cutting open between tracheas. The unwanted body parts, such as the gut and fat tissue, were removed without harming muscles, brain and nerve bundles. Then the larval body was spread to all sides by placing pins on all four corners of the body, exposing ventral muscles. Remaining unnecessary tissue of fat, gut and trachea were removed and the dissected neuromuscular system was washed with HL-3 solution.

4.1.4. Immunohistochemistry of Larval Neuromuscular System

After fixation of the collected organs in 3.7% formaldehyde in HL-3 for 20 minutes, fixation solution was washed twice with HL-3 for 10 min each. After carefully removing the pins, larvae were moved into centrifuge tube with 1 ml PBX4 solution and washed every 15 min four times. Then the samples were blocked for two hours in 10% NGS in PBX4 at room temperature and primary antibodies were added for overnight incubation at 4ºC.

The next morning, primary antibody solution was removed and the samples were washed five times for 10 min with 1 ml PBX4. The samples were incubated in blocking solution after adding proper amounts of secondary antibodies for two hours at room temperature in darkness. After incubation with secondary antibody, the samples were washed with PBX4 eight times for 15 min. Then the samples were placed on a drop of mounting medium on microscopy slide with the same orientation. After organizing the organs, a cover slip was placed on top and all four sides were sealed with nail polish. Prepared slides were kept at 4°C. For visualization, Leica confocal microscope with LAS

AF software was used. The images obtained were processed and analyzed using ImageJ software.

4.2. Molecular Biology Methods

4.2.1. Isolation of Plasmids

Plasmids were isolated using GeneJET Plasmid Miniprep Kit (Thermo Scientific) according to the supplied protocol. Major steps of the protocol include growing bacterial cultures for 16 hours at 37°C in LB medium on a shaker. 2 ml (10 ml for low copy number plasmids) culture was centrifuged at 6800 G for 2 min. After discarding the supernatant, the pellet was resuspended in 250 µl of resuspension buffer. Then 250 µl of lysis buffer was added and the tube was inverted 6 times for mixing. After incubation for up to 5 min at room temperature, 350 µl of neutralization buffer was added. After gently inverting the mixture 6 times, the samples were centrifuged at maximum speed (>13000 rpm) for five minutes. Supernatant was collected in spin columns provided with the kit. Spin column was centrifuged for 1 min each once for binding, twice with 500 µl of wash solution for washing, once for discarding extra ethanol. After placing 50 µl of EB in the center of the column with a pipette, the column was incubated at room temperature for 2 min and centrifuged for 2 min at maximum speed to collect the plasmid DNA, which was kept at -20°C after measuring its concentration using NanoDrop spectrophotometer.

4.2.2. Transformation of Plasmid DNA

Escherichia coli (*E. coli*) propagated from commercially available chemocompetent cells (TOP10) cells were previously made competent using Rubidium Chloride (RbCl). After thawing 50-100 µl of these competent cells on ice for 5 minutes, up to 5 µl of ligation product or 1 µl of purified plasmid was added to the cells. The cells were incubated on ice for 30 min and they were heat shocked in water bath for 90 seconds at 42°C. After keeping them on ice for 5 more min, 950 µl of SOC medium (at 37°C) was added to and the cells were recovered by shaking at 37°C for one hour. 100 µl of recovered culture was spread on LB plates with the right antibiotic for overnight growth at 37°C.

4.2.3. Restriction Digestion

All of the digestions were done according to the used enzyme's protocol. Unless otherwise is stated the following setup in Table 4.1 was used. 1 µg of DNA is cut in 15 minutes at 37 °C unless otherwise is stated in the protocol.

Table 4.1. Restriction digestion setup.

Component	**Volume (µl)**
dH_2O	12
10X FastDigest Green buffer	2
Plasmid DNA (200 ng/µl)	5
FastDigest enzyme	1
Total	20

4.2.4. DNA Isolation From Agarose Gel

After samples were run on 1% agarose gel prepared with 1X TAE, the bands were visualized under UV. The right band was cut as small as possible using a clean scalpel and Agarose Gel DNA Extraction Kit (Roche) was used to isolate DNA from the cut band.

4.2.5. Ligation

For ligation of two DNA fragments with sticky ends, the following setup (Table 4.2) was used to prepare the reaction and the product's (T4 DNA ligase, Thermo Scientific) protocol was used.

Unless otherwise is stated, 1:2 molar ratio was used for vector:insert and volume of vector and insert were calculated according to their lengths and concentrations to achieve a 1:2 molar ratio. If necessary amount of vector was lowered to 20 ng in order to keep the vector:insert ratio. The reaction was prepared in a 0.2 ml tube and incubated at 22°C for 60 min.

Table 4.2. Ligation reaction setup.

Component	**Volume (µl)**
dH_2O	Up to total volume of 20
10X T4 DNA Ligase Buffer	2
Vector	100 ng
Insert	1:2 molar ratio
T4 DNA ligase (5u/µl)	0.2
Total	20

4.2.6. Purification After Reactions

If it is necessary to clean up DNA from enzymes and buffers for next steps which may be affected by such contaminants, GeneJet PCR Purification kit (Thermo Scientific) was used according to the product's protocol.

4.2.7. High Fidelity PCR

For high fidelity PCR, Phusion High-Fidelity DNA Polymerase was used to prepare the reaction mix of 20 µl as found in Table 4.3.

Table 4.3. High Fidelity PCR Setup.

Component	**Volume (µl)**
dH_2O	12.4
5X Phusion Buffer	4
Template DNA (100 ng/µl)	1
dNTP (10 mM)	0.4
Forward primer (10 µM)	1
Reverse primer (10 µM)	1
Phusion DNA Polymerase	0.2

For amplification the following conditions are used unless otherwise is stated in the text (Table 4.4).

Table 4.4. Cycling Conditions For High Fidelity PCR.

Cycle	**Step**	**Temperature (°C)**	**Duration (s)**
1	Initial Denaturation	98	30
25	Denaturation	98	10
	Annealing	45-72	15
	Elongation	72	30 per kb
1	Final Elongation	72	300
1	Hold	4	hold

4.2.8. Colony PCR

For colony PCR *Taq* DNA Polymerase Recombinant (Thermo Scientific) was used to prepare the reaction mix as found in Table 4.5.

Table 4.5. Colony PCR Setup.

Component	**Volume (µl)**
dH_2O	12.9
10X Taq Buffer	2
25 mM $MgCl_2$	1.6
Picked colony in suspension	1
dNTP (10 mM)	0.4
Forward primer (10 µM)	1
Reverse primer (10 µM)	1
Taq DNA Polymerase (5 u/µl)	0.1

Before preparing the reaction, a single colony was picked using a pipette tip and immersed in sterile dH_2O by pipetting up and down. This suspension was kept at 4°C for later use in transformation or repeat of the PCR. Bacteria stay alive for at least one week in this condition.

For amplification the following conditions are used unless otherwise is stated in the text (Table 4.6).

Table 4.6. Cycling Conditions For Colony PCR.

Cycle	**Step**	**Temperature (°C)**	**Duration (min)**
1	Initial Denaturation	95	5
25	Denaturation	95	0.5
	Annealing	45-72	0.5
	Elongation	72	1 per kb
1	Final Elongation	72	5
1	Hold	4	hold

4.2.9. Site Directed Mutagenesis

In order to do site-directed mutagenesis, plasmid was amplified using *Pfu* polymerase with primers containing the mutation. The PCR product was digested with *Dpn*I restriction enzyme, which degrades methylated DNA, thus PCR product was not affected.

For PCR *Pfu* Ultra High Fidelity DNA Polymerase Recombinant (Agilent) was used to prepare the reaction mix as found in Table 4.7.

Table 4.7. Site-directed Mutagenesis PCR Setup.

Component	**Volume (µl)**
dH_2O	To 50
10X *PfuUltra* HF Buffer	5
dNTPs (10 mM)	1
DNA template (100 ng/µl)	0.5
Forward primer (100 ng/µl)	125 ng
Reverse primer (100 ng/µl)	125 ng
PfuUltra DNA Polymerase (2.5 u/µl)	1

For amplification the following conditions are used unless otherwise is stated in the text (Table 4.8).

Table 4.8. Cycling Conditions For Site-directed Mutagenesis PCR.

Cycle	Step	Temperature (°C)	Duration (min)
1	Initial Denaturation	95	2
12	Denaturation	95	0.5
	Annealing	55	0.5
	Elongation	68	1 per kb
1	Hold	4	hold

After the amplification steps, PCR tube is placed on ice. 1 µl (20 u) of *Dpn*I (New England Biolabs) is added to the tube and incubated at 37°C for an hour. The product is purified as described in Section 4.2.6 and 5 µl of the purified sample is used to transform bacteria as described in Section 4.2.2.

4.3. *Drosophila* Crosses

4.3.1. Crosses for Mobilization of *Minos* Elements

After obtaining commercially available lines for *Minos* element in *CG4623* and *Minos* Transposase these alleles were balanced using TM2 and sp. Then, the balanced lines were crossed with each other to bring *Minos* element and *Minos* transposase together in the same genotype (Figure 4.1). Two days after setting up the cross, flies were transferred to a new vial and the old vials were heat-shocked daily for one hour at 37°C until pupariation.

$$\text{♀}\ \frac{y,w}{w};\frac{sp}{+};\frac{Mi[ET1]CG4623[MB07860]}{TM2}\ \text{X}\ \frac{y,w}{-};\frac{sp}{\text{SM6a, P[w[+mC]=hsILMiT]2.4}};\frac{TM2}{+}\ \text{♂}$$

$$\downarrow$$

$$\text{Select ♀ / ♂}\ \frac{SM6a,\ P\{w[+mC]=hsILMiT\}2.4}{sp/+};\frac{Mi\{ET1\}CG4623[MB07860]/\Delta}{TM2}$$

Figure 4.1. Generation of *Minos* mobilization line.

The obtained mosaic flies were selected using GFP marker in the eye under GFP scope and were crossed to a quadruple balancer bearing fly for selecting only Minos deletion (Figure 4.2).

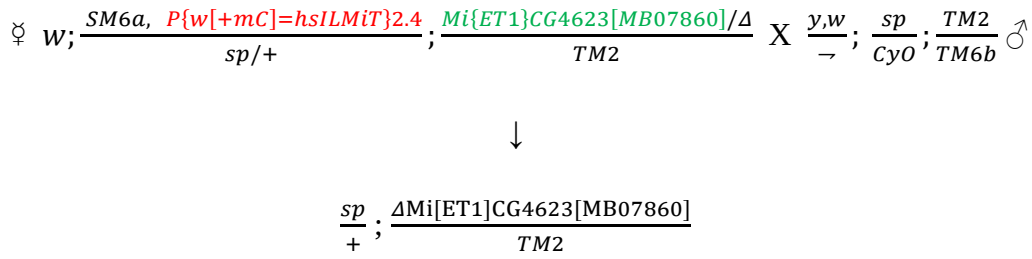

Figure 4.2. Selection of *Minos* deletion.

Stocks for each deletion allele were obtained by crossing with quadruple balancer bearing fly again (Figure 4.3).

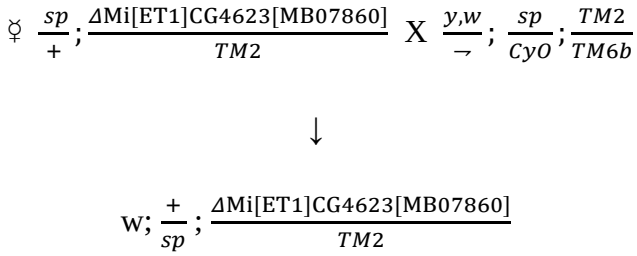

Figure 4.3. Cross for generating stocks of deletion alleles.

4.3.2. Crosses for Analysis of Mitochondrial Dynamics

As the RNAi lines (UAS-Drp1-RNAi and UAS-Marf-RNAi) are homozygous, the two lines and their control (y, v) were crossed to the motor neuron driver with mitochondrially tagged GFP (D42-GAL4, UAS-mitoGFP/TM6b) and selection for GFP signal and against tubby character (TM6b) was performed.

5. RESULTS

5.1. Overexpression of *CG4623*

As there was no commercially available overexpression line to express *CG4623* spatiotemporally, it was necessary to generate a UAS-*CG4623* line in order to understand the function of this gene.

5.1.1. Generation of an Overexpression Construct for *CG4623*

For spatiotemporal overexpression of *CG4623*, a construct for UAS-*CG4623* was generated. For this purpose, the open reading frame (ORF) of *CG4623* was cloned into the P-element based UAS vector with attachment sites, pUASTattB. The construct was prepared to allow site-specific integration of *CG4623*-ORF into the *Drosophila* genome using *ΦC31* integrase.

CG4623 cDNA (RE69232) was obtained from the Drosophila Genomics Resource Center (USA) and its ORF was amplified using primers that had *Xba*I and *Xho*I restriction sites, in order to clone the ORF into the pUASTattB vector. For the amplification of the ORF, high fidelity PCR with 35 cycles at an annealing temperature of 54°C, and the primers CG4623_pUAST_FP and CG4623_pUAST_RP were used. The PCR product was run on a 1% agarose gel (1X TAE) and the expected band of 998 bp was purified from the gel (Figure 5.1a).

The purified fragment was ligated to pGEM-T Easy vector (Promega, USA). After transformation into RbCl competent cells (*Escherichia coli*), the recovered culture was plated on LB plates with ampicillin. The next morning, single colonies were picked and colony PCR with 30 cycles at an annealing temperature of 50°C was set up using T7 and SP6 primers, which are present on the pGEM-T Easy backbone. The PCR products for the selected colonies were run on a 1% agarose gel (1X TAE) and the expected band of 1173 bp was observed for all of the colonies (Figure 5.1b). Nine selected colonies were grown in LB liquid media with ampicillin for 16 hours and plasmids were extracted afterwards.

The plasmids obtained for each positive colony was digested with the restriction enzyme *EcoR*I and loaded on a 1% agarose gel (1X TAE). The expected fragment sizes of this analytical digestion were 2997, 386, 363 and 267 bp. For all of the plasmids, an undigested sample was also loaded and for all of the *EcoR*I-digested plasmids the expected pattern was observed though the small fragments (386, 363 and 267 bp) were not discernible as separate bands due to their close size (Figure 5.1c). After colony PCR and analytical digestion, as the third form of verification, plasmids were Sanger sequenced using T7 and SP6 universal primers and sequencing results were analyzed using ApE A Plasmid Editor. Out of six clones, one of the mutation-free constructs was selected for further experiments and named XhoI-CG4623-XbaI-pGEM-T Easy (Figure 5.1e).

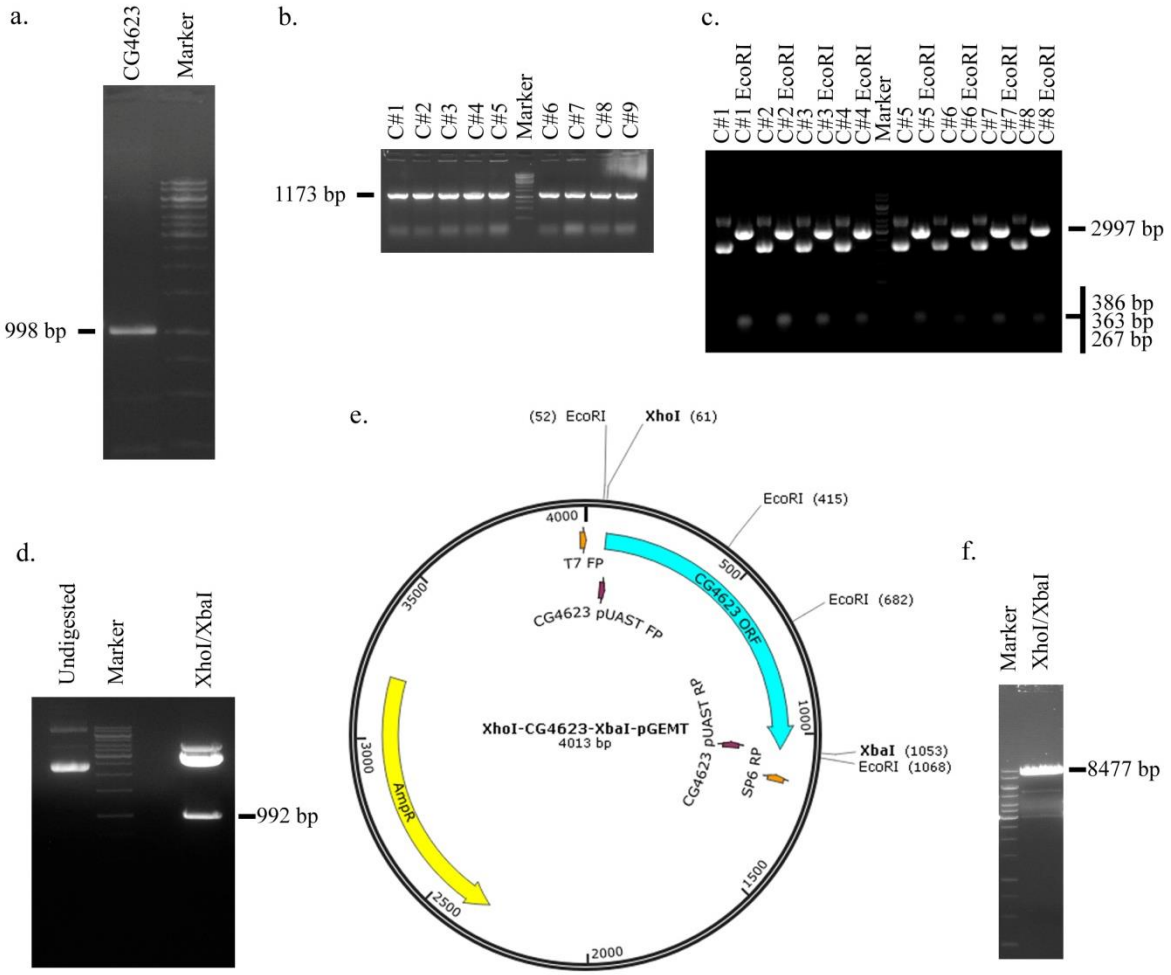

Figure 5.1. Cloning of *CG4623* ORF into pUASTattB. (a) High fidelity PCR of *CG4623*, (b) colony PCR, (c) analytical digestion, (d) digestion for cloning and (e) vector map of Xho-CG4623-XbaI pGEMT-easy construct, and (f) pUASTattB restriction digestion.

XhoI-CG4623-XbaI-pGEM-T Easy was double digested with the restriction enzymes *Xho*I and *Xba*I for cloning into the pUAST vector and loaded on a 1% agarose gel (1X TAE) (Figure 5.1d). The digestion was not complete as the band for partially digested plasmid was also observed; however, the expected double digested fragment of 992 bp was purified from the gel. pUASTattB vector was also cut with the same restriction enzymes and loaded on a 1% agarose gel (1X TAE). The expected bands were 8477 and 12 bp, corresponding to the backbone and part of the multiple cloning site (MCS), respectively (Figure 5.1f).

The digested pUASTattB backbone and *XhoI-CG4623-XbaI* fragment were ligated and the ligation product was transformed into competent cells. Single colonies were picked after growth overnight and colony PCR was performed with primers on the pUASTattB backbone (pUAST_seq_FP and pUAST_seq_RP) with 30 cycles and an annealing temperature of 51°C. After running the products on a 1% agarose gel (1X TAE), positive colonies that gave a band of 1179 bp were selected (Figure 5.2a). The first ten positive colonies were grown in LB liquid media with ampicillin for 16 hours and the plasmids were isolated. According to the map of the construct (Figure 5.2b), analytical digestion was performed with *BamH*I. After running the products on a 1% agarose gel (1X TAE), it was observed that all of the colonies were positive for the insert and gave two fragments of 7358 and 2111 bp (Figure 5.2c). The plasmids were sequenced using pUASTattB backbone primers (pUAST_seq_FP and pUAST_seq_RP), and sequences were analyzed using Ape A Plasmid Editor. One of the mutation free construct out of six was selected for further studies.

As *CG4623*-pUASTattB construct has a critical importance in further studies, not only the MCS and the insert were sequenced using primers on the backbone but also the restriction digestion patterns using different enzymes were checked before injecting *CG4623*-pUASTattB into *Drosophila* embryos. The products for double digestions with *EcoR*I/*Nhe*I (expected bands: 8383, 397, 382 and 267 bp), *Xba*I/*Nhe*I (expected bands: 8012 and 1417 bp), *Xho*I/*Nhe*I (expected bands: 9004 and 425 bp) and digestions with *Sac*I (expected bands: 5748 and 3721 bp), *Sma*I (expected bands: 5253 and 4216 bp) and *Sac*II (expected bands: 7731 and 1738 bp) were run on a 1% agarose (1X TAE) (Figure 5.2d-e).

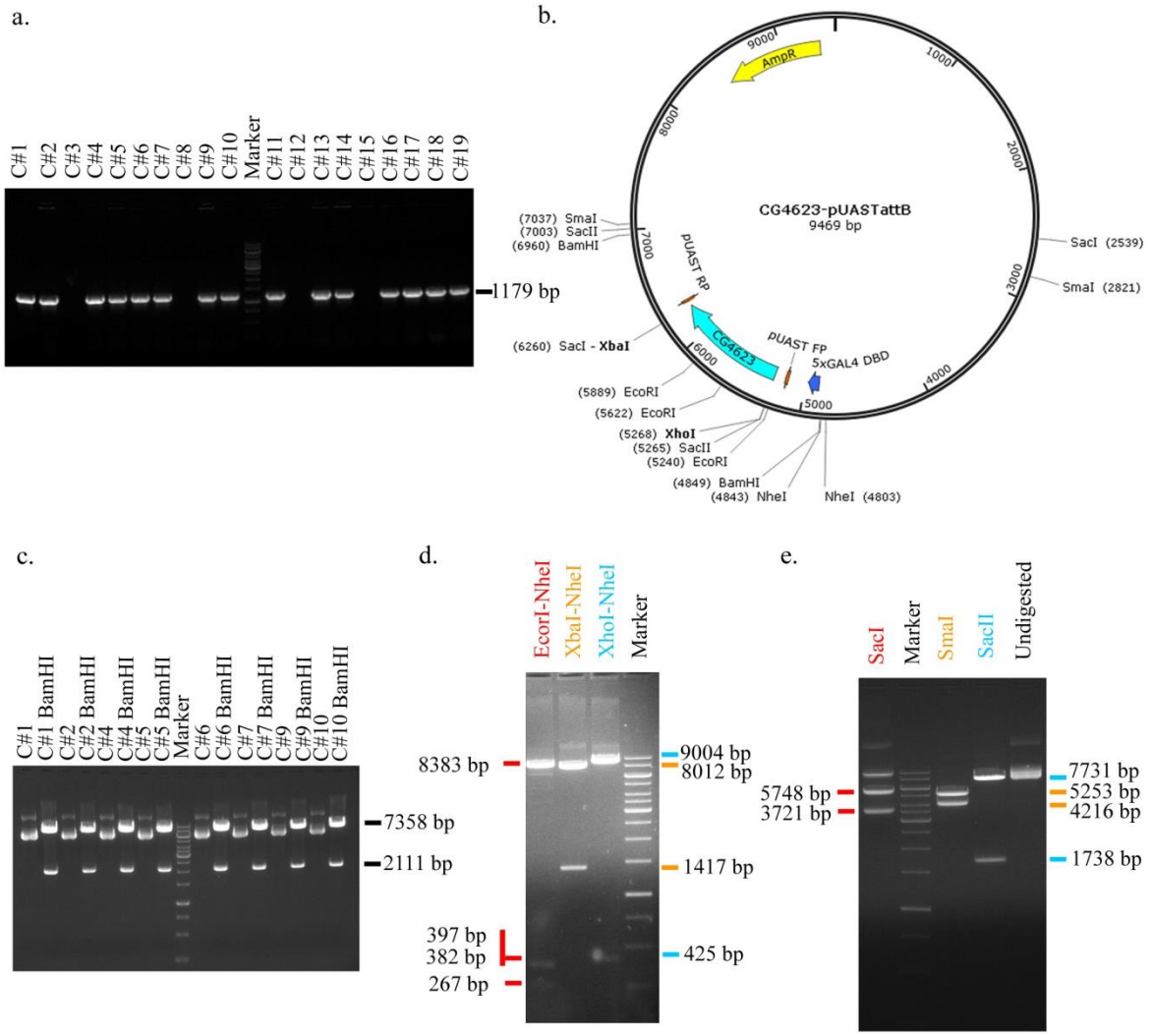

Figure 5.2. Verification of *CG4623*-pUASTattB construct. (a) Colony PCR, (b) vector map and analytical digestions with (c) *BamH*I, (d) *EcoR*I/*Nhe*I, *Xba*I/*Nhe*I, *Xho*I/*Nhe*I (e) *Sac*I, *Sma*I, *Sac*II for *CG4623*-pUASTattB

5.1.2. Generation of a Transgenic Overexpression Line for *CG4623*

After the *CG4623*-pUASTattB construct sequence was verified using eight different restriction enzymes, colony PCR and Sanger sequencing using primers on the vector backbone, it was isolated in large amounts without freezing to prevent freeze-thaw degradation. It was sent to an injection company for *ΦC31* integrase-mediated site-specific transgenesis (Genetivision, USA). The landing site for the construct was chosen as the *attP2* site that resides on the left arm of the third chromosome (3L, specifically 68A4). After injection, three independent fly lines were obtained and balanced with TM3.

5.2. Generation of *CG4623* Partial Deletion Alleles Using *Minos* Elements

As part of understanding the function of *CG4623*, analysis of not only the spatio-temporal overexpression, but also the loss of *CG4623* was important. Among commercially available fly stocks, there was no a line that included partial or full deletion of *CG4623* without interrupting neighboring genes. The best available option was to analyze Df(3L)Exel6103 line from the Exelixis defiency collection. This fly line had a heterozygous deletion on the left arm of the third chromosome between 64C4 and 64C8, which included *CG4623* (64C7) along with nearly twenty other genes.

As it was necessary to delete or interrupt *CG4623* without affecting other genes, instead of a deficiency line, we aimed to mobilize a transposable element near or on *CG4623* in order to generate partial or full deletion of the gene. The only suitable transposable element was a *Minos* element located near the 3' end of the first intron of *CG4623*, in the 5' direction (Figure 5.3a). This *Minos* element was chosen to generate a partial deletion allele since these transposons can cause deletions of flanking sequences when they excise out (Metaxakis *et al*., 2005).

As described in the Methods, crosses for mobilizing the *Minos* element were set up. The selection of EGFP-mosaic flies carrying Minos excisions in some of their cells was performed using a Fluorescent Dissection Microscope with a GFP filter in comparison to the *Minos* transposase line as negative control (Figure 5.3b) and *Minos* element line as positive control (Figure 5.3c). Since the mosaic flies for the *Minos* element had a distinct eye phenotype with patchy EGFP expression (Figure 5.3d) they were easily selected. After balancing crosses, 76 lines were screened for *Minos* element excision by fly genomic PCR using primers (CG4623_Upstream_Seq and CG4623_Downstream_Seq) that are more than 1.3 kb away from the *Minos* element insertion site. After running the PCR products on a 1% agarose gel (1X TAE), the expected band of 2731 bp for a precise excision and a non-specific band near 900 bp were observed for all of the lines screened, except for those not producing any bands, suggesting inefficient genomic DNA extraction (Figure 5.3e).

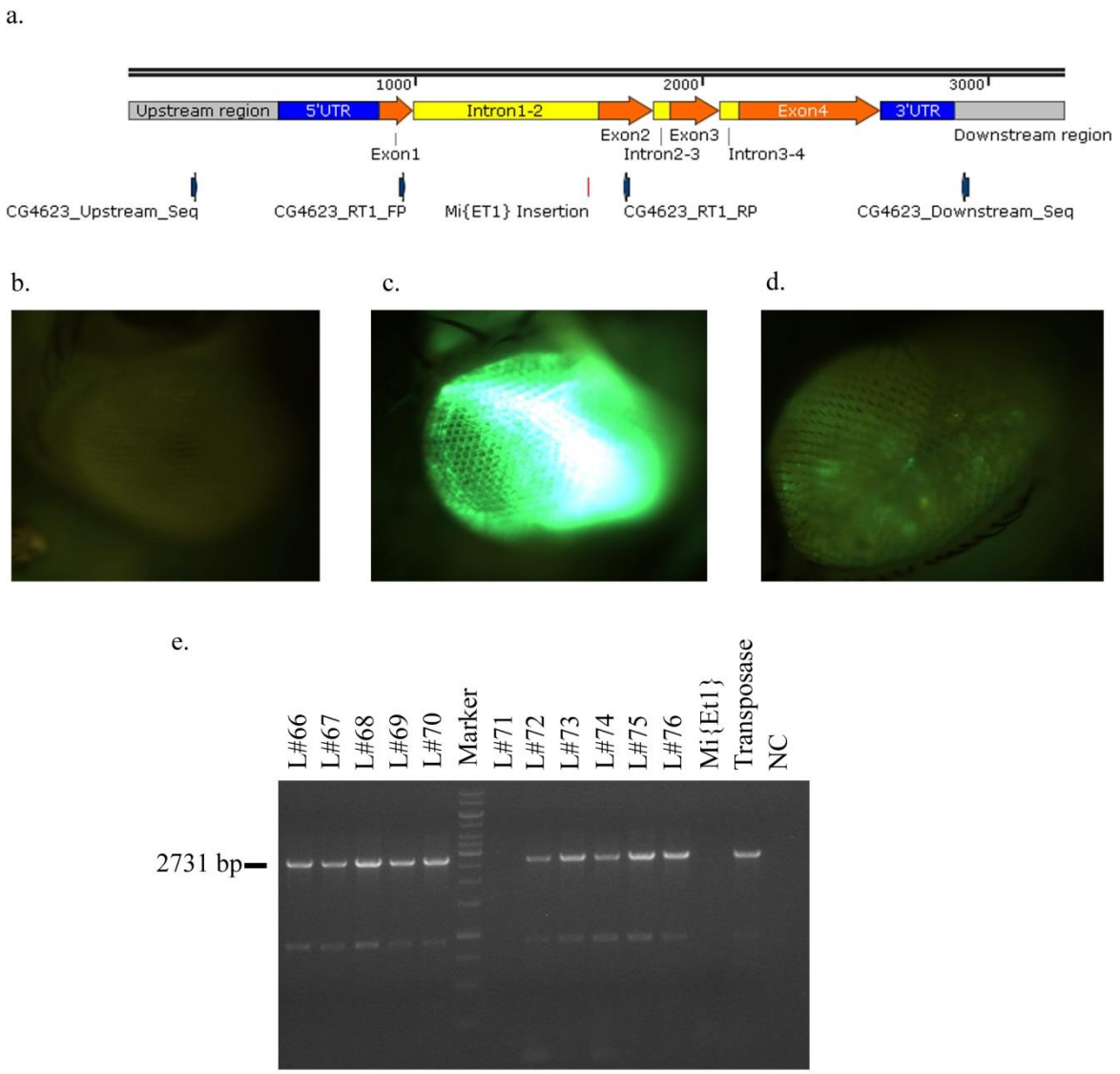

Figure 5.3. Mobilization of the *Minos* element on *CG4623*. (a) *CG4623* map and *Minos* element, the eye of living fly visualized with GFP filter carrying (b) *Minos* transposase, (c) *Minos* element and (d) mosaic for *Minos* element, (e) *Minos* excision PCR screen.

5.3. *GDAP1* Knock-in Constructs

The constructs for knocking-in of wildtype *GDAP1* cDNA and CMT-causing mutant forms of *GDAP1* were generated using the pABC vector. This vector has *attB* sites flanking its MCS to allow site-specific knock-in of any fragment in place of *CG4623* by integrase-mediated approach

5.3.1. Generation of Wildtype Human *GDAP1* Knock-in Constructs

In order to knock-in human *GDAP1* in place of *CG4623* using IMAGO system, a *GDAP1*-pABC construct was generated. First, *GDAP1* cDNA for transcript variant 1 (NM_018972.2, Origene SC317569) was amplified with high fidelity PCR using primers that have *BamH*I and *Hind*III restriction sites (GDAP1_pABC_FP and GDAP1_pABC_RP) using 35 cycles with an annealing temperature of 54°C. The product was run on a 1% agarose gel (1X TAE) and the expected fragment of 1088 bp was purified and ligated into the pGEM-T Easy vector (Figure 5.4a).

After transformation of competent cells, the recovered culture was plated on LB with ampicillin. Following growth for 16 hours, colony PCR was performed for ten picked colonies using T7 and SP6 primers for 30 cycles with an annealing temperature of 50°C (Figure 5.4b). The four positive colonies giving bands of 1263 bp were used to inoculate LB media and plasmids isolated from these were sent to Sanger sequencing using T7 and SP6 primers.

From the four sequenced clones, one of the mutation free clones was selected and the plasmid was digested with *BamH*I and *Hind*III (Figure 5.4c-d). The expected bands of 3021 and 1083 bp were observed and the *BamH*I-*GDAP1*-*Hind*III fragment (1083 bp) was purified from a 1% agarose gel (1X TAE). The *atonal*-pABC construct was also digested with *BamH*I and *Hind*III to obtain the pABC backbone of 2761 bp, running along with the other two fragments of 701 and 282 bp for *atonal* on a 1% agarose gel with 1X TAE (Figure 5.4e) (Choi *et al*., 2009). The backbone was purified from the gel and ligated to the *BamH*I-*GDAP1*-*Hind*III fragment. The transformed competent cells were plated on LB ampicillin plates and grown overnight.

After selecting single colonies, colony PCR was performed using primers on the pABC backbone (pABC_seq_FP and pABC_seq_RP) for 30 cycles with an annealing temperature of 54°C. The PCR products were run on a 1% agarose gel (1X TAE) and positive colonies, yielding a band of 1413 bp were selected for growth in LB media with ampicillin for 16 hours (Figure 5.5a).

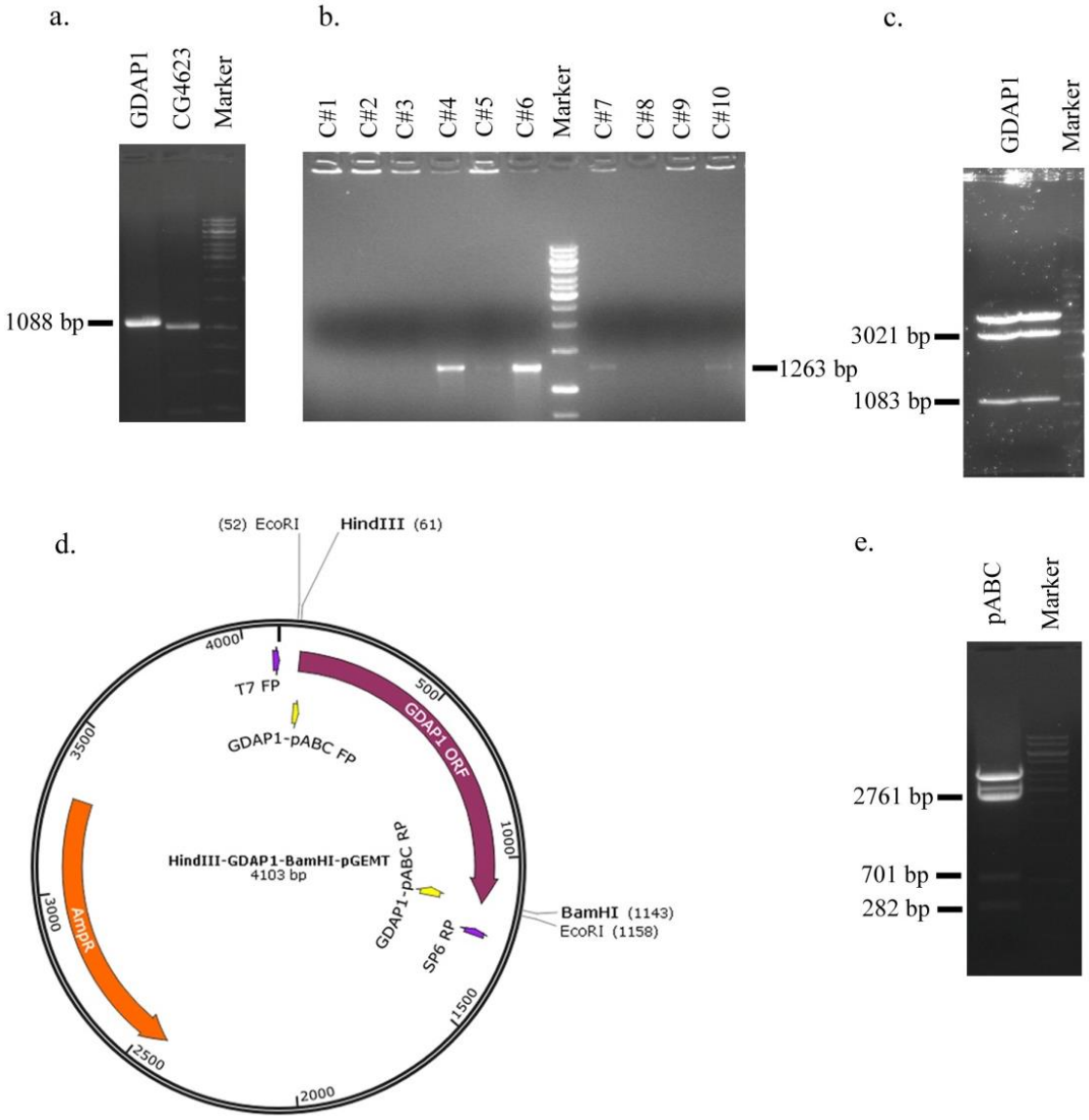

Figure 5.4. Preparation of *GDAP1* knock-in construct. (a) High fidelity PCR for *GDAP1*, (b) Colony PCR, (c) *BamH*I and *Hind*III digestion and (d) vector map for *Hind*III-*GDAP1*-*BamH*I-pGEM-T easy construct, (e) *BamH*I and *Hind*III digestion of *atonal*-pABC.

After plasmids were isolated for five positive colonies, *Sma*I, an enzyme that cuts only the *attB* sites flanking the MCS was used for analytical digestion (Figure 5.5b). The PCR for the clones was repeated using the primers on the backbone of the vector (pABC_seq_FP and pABC_seq_RP) for 30 cycles at an annealing temperature of 54°C. The *Sma*I digestion and PCR products were run on 1% agarose gel (1X TAE) and expected bands of 2702 and 1141 bp, and 1413 bp were observed, respectively (Figure 5.5c).

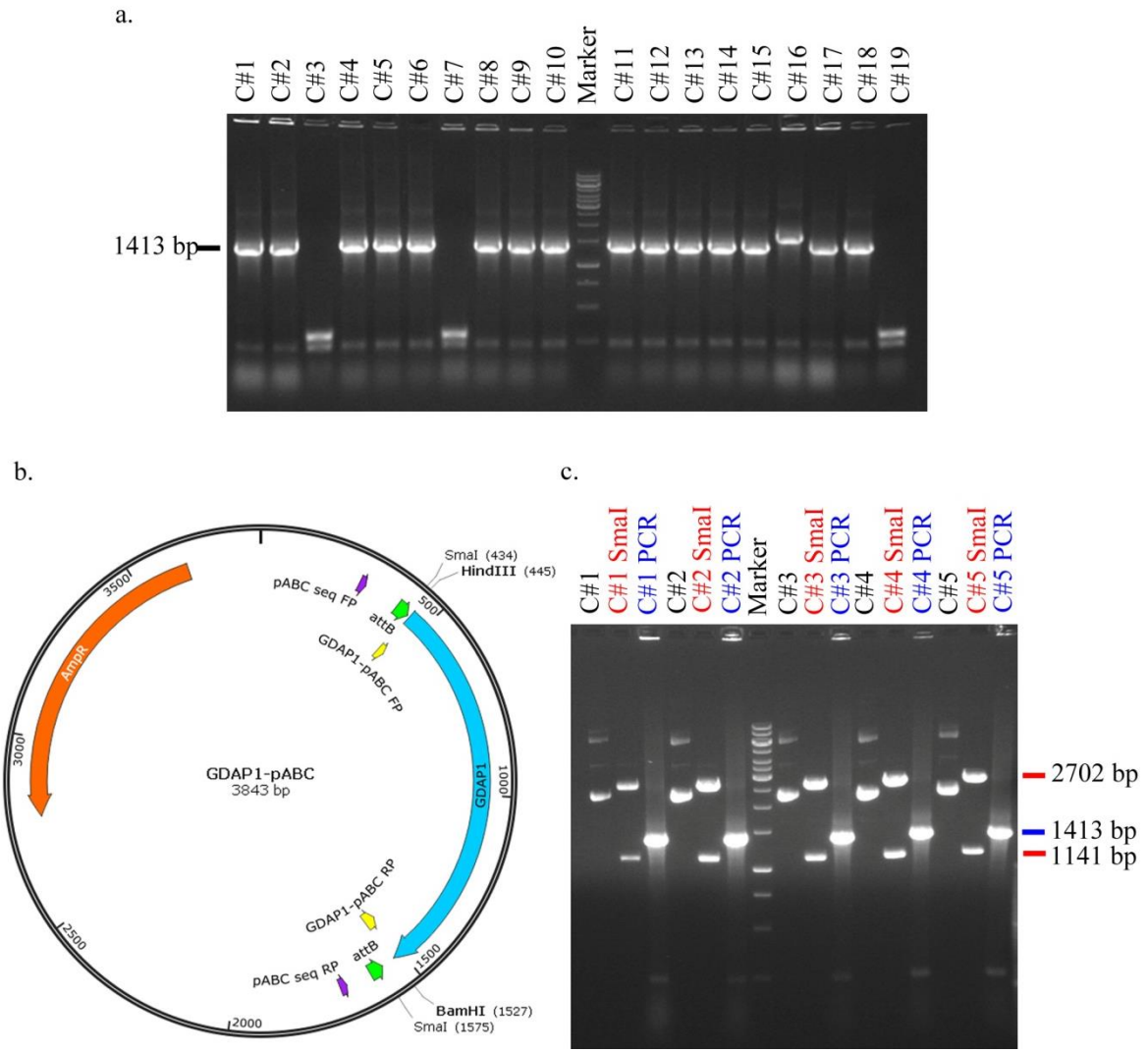

Figure 5.5. Verification of *GDAP1*-pABC knock-in construct. (a) Colony PCR, (b) vector map and (c) analytical digestion with *Sma*I and PCR results for *GDAP1*-pABC.

All of the five positive clones were sent to Sanger sequencing using sequencing primers on the backbone (pABC_seq_FP and pABC_seq_RP). One of the mutation free clones was selected for knock-in using *ΦC31* integrase mediated transgenesis into *CG4623* knock-out flies in the future.

5.3.2. Selection of CMT Causing Mutations for Knock-in

Out of many CMT-causing mutations of *GDAP1*, nine non-synonymous mutations with various phenotypes were selected to be modeled in flies, according to axonal, intermediate and demyelinating characteristics, segregation pattern, conservation in

Drosophila, severity of the phenotype and domain they are located on (Table 5.1 and Figure 5.6).

Table 5.1. Selected CMT mutations to be modeled in flies. WI: walking independently; WS: walking with support; WB: wheelchair bound; IE: inexcitable; ND: not determined; AX: axonal; DM: demyelinating; INT: intermediate; Dom: dominant; Rec: recessive; p: people; y: years (Cassereau *et al*., 2011).

Mutation/ Domain	**Phenotype/ Inheritance**	**Number of Patients**	**Onset (y)**	**Walking Ability**	**MNCV (m/s)**	**CMAP (mV)**	**Histo-logy**
P78L GST-N	INT Rec	4 (2 families)	<2	WS: 8-15 y (2 p) WB: 6-15 y (2 p)	13.2-24.5 (7-8 y)	0.3-0.4	ND
R120Q α4	DM Rec	1	2	ND	IE	IE	AX/DM
R120W α4	AX Dom	2	10-20	WI: 35 y	Normal (35 y)	Normal (35 y)	ND
D149Y None	INT Rec	1	3	WB: 60 y	IE (63 y)	IE	AX/DM
P153L α4-α5 loop	INT Rec	1 1	3.5 1	WB: 27 y ND	31 (5 y) IE	0.15 IE	AX (5 y) ND
T157P α4-α5 loop	AX Dom	1	1	WI: 10 y	45	15	ND
C240Y GST-C	AX Dom	3	10-50	WI: 70-80 y (2 p) WS: 50 y	>50	6-15	ND
G271R (+R120W) GST-C	AX Rec	1	3	WB: 20 y	19	0.3	ND
Y279C α7/GST-C	AX Rec	4 3	3-8 1-5	WS: 32 y WB: 10-20 y (3 p) WS: 5, 36, 50 y	IE (19-22 y) 43,5 (2.5 y)	IE 1.3	ND ND

Among these mutations, P78L, P153L, G271R and Y279C correspond to a residue that is conserved in *Drosophila melanogaster*. Except for G271R, all of the mutations were either segregating as recessively or dominantly. The R120W mutation, on the other hand,

is a dominant mutation causing mild phenotype, but in compound heterozygous state with the G271R mutation, it causes a severe phenotype with early onset (Ammar *et al*., 2003).

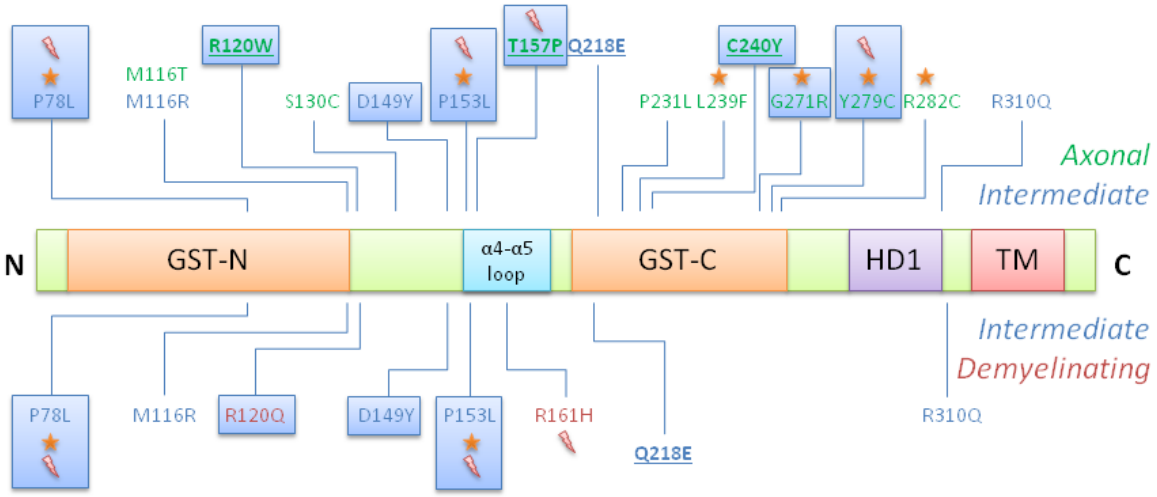

Figure 5.6. Selected CMT-causing missense mutations of *GDAP1* to be knocked-in. Underlined: dominant; Star symbol: conservation in *Drosophila melanogaster*; thunder symbol: severe phenotype; mutations in blue rectangles: selected (Cassereau *et al*., 2011).

5.3.3. Generation of CMT Causing Mutant *GDAP1* Knock-in Constructs

Using the generated *GDAP1*-pABC construct as the template, nine mutant forms of *GDAP1*-pABC were generated by site-directed mutagenesis as described in the Methods. The same quantity (125 ng each) of primers (Table 5.2), cycle number (12) and annealing temperature (55°C) was used in all site-directed mutagenesis PCR. After site-directed mutagenesis, *Dpn*I digestion, purification, transformation and growth on LB-agar with ampicillin, colonies were picked for inoculating LB media. Plasmids were isolated and sent to Sanger sequencing using primers on the backbone (pABC_seq_FP and pAB_seq_RP). Parts of the chromatograms of mutant *GDAP1*-pABC constructs corresponding to the mutated residue are marked in Figure 5.7.

Table 5.2. Primers used in generating mutant forms of *GDAP1* in pABC vector.

Construct	Primer Pair
P78L	GDAP1_pABC_P78L_FP and GDAP1_pABC_P78L_RP
R120Q	GDAP1_pABC_R120Q_FP and GDAP1_pABC_ R120Q_RP

Table 5.2. Primers used in generating mutant forms of *GDAP1* in pABC vector. (cont.)

R120W	GDAP1_pABC_R120W_FP and GDAP1_pABC_ R120W_RP
D149Y	GDAP1_pABC_D149Y_FP and GDAP1_pABC_ D149Y_RP
P153L	GDAP1_pABC_P153L_FP and GDAP1_pABC_ P153L_RP
T157P	GDAP1_pABC_T157P_FP and GDAP1_pABC_ T157P_RP
C240Y	GDAP1_pABC_C240Y_FP and GDAP1_pABC_ C240Y_RP
G271R	GDAP1_pABC_G271R_FP and GDAP1_pABC_ G271R_RP
Y279C	GDAP1_pABC_Y279C_FP and GDAP1_pABC_ Y279C_RP

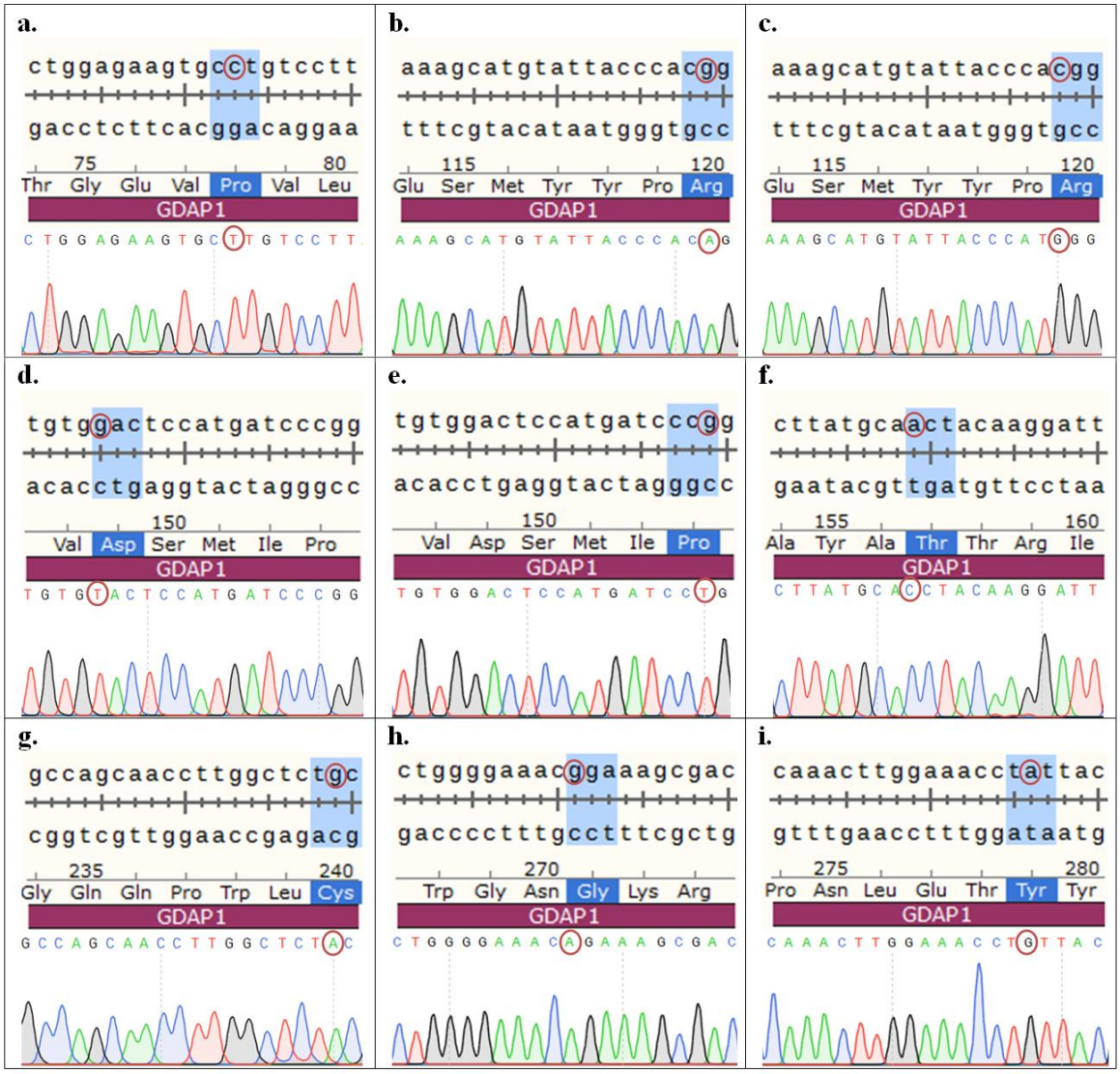

Figure 5.7. Generation of CMT causing mutant *GDAP1* knock-in constructs. Sanger sequencing results after site-directed mutagenesis for *GDAP1*-pABC with (a) P78L, (b) R120Q, (c) R120W, (d) D149Y, (e) P153L, (f) T157P, (g) C240Y, (h) G271R, (i) Y279C.

The prepared constructs are ready for knock-in using *ΦC31* integrase-mediated transgenesis to the *CG4623* knock-out flies, when they are generated.

5.4. Understanding *CG4623* Expression Pattern

In order to compare CG4623's function to GDAP1, it is necessary to know the expression pattern of CG4623. However, there are no available antibodies against CG4623 to visualize the expression of the protein. Thus, the aim of this part of the thesis was to generate *CG4623*-GAL4 driver and *CG4623*-mCherry reporter lines and production of antibodies against CG4623.

5.4.1. Generation of Knock-in Construct for *CG4623*-GAL4 Driver

As downstream and upstream regulatory elements are thought to be unaffected during knockout of *CG4623*, replacing this gene with the coding sequence of GAL4 would allow generation of a *CG4623*-GAL4 driver. Crossing this line with any UAS responder line is expected to produce progeny that will be able to mimic the expression pattern of the gene.

After high fidelity PCR for GAL4 coding sequence with primers that have *Hind*III and *Kpn*I restriction sites (GAL4_ pABC_FP and GAL4_ pABC_RP) with 25 cycles and annealing temperature of 55°C, the product was run on a 1% agarose gel (1X TAE) and the band corresponding to *GAL4* (2664 bp) was purified from the gel (Figure 5.8a). The purified fragment was digested with *Kpn*I and *Hind*III enzymes and purified again without loading on a gel. Using the same enzymes, the *GDAP1*-pABC construct was digested to obtain the pABC backbone corresponding to the 2740 bp band on a 1% agarose gel (1X TAE) and it was purified from the gel (Figure 5.8b). The *Hind*III-GAL4-*Kpn*I fragment was ligated to the pABC backbone that is digested with the same enzymes (Figure 5.8c).

After transformation, plating on LB agar with ampicillin and overnight growth, colonies were selected for colony PCR. Colony PCR was performed using primers on pABC (pABC_seq_FP and pABC_seq_RP) for 30 cycles with an annealing temperature of 54°C. After running the products on a 1% agarose gel (1X TAE), positive colonies,

corresponding to the 2962 bp band, were selected (Figure 5.8d). Plasmids were isolated from these positive clones and analytical digestion with *Kpn*I and *Xho*I was performed to verify the length of the constructs. The restriction digestion products run on a 1% agarose gel (1X TAE) gave the expected pattern of 2963 and 2429 bp (Figure 5.8e).

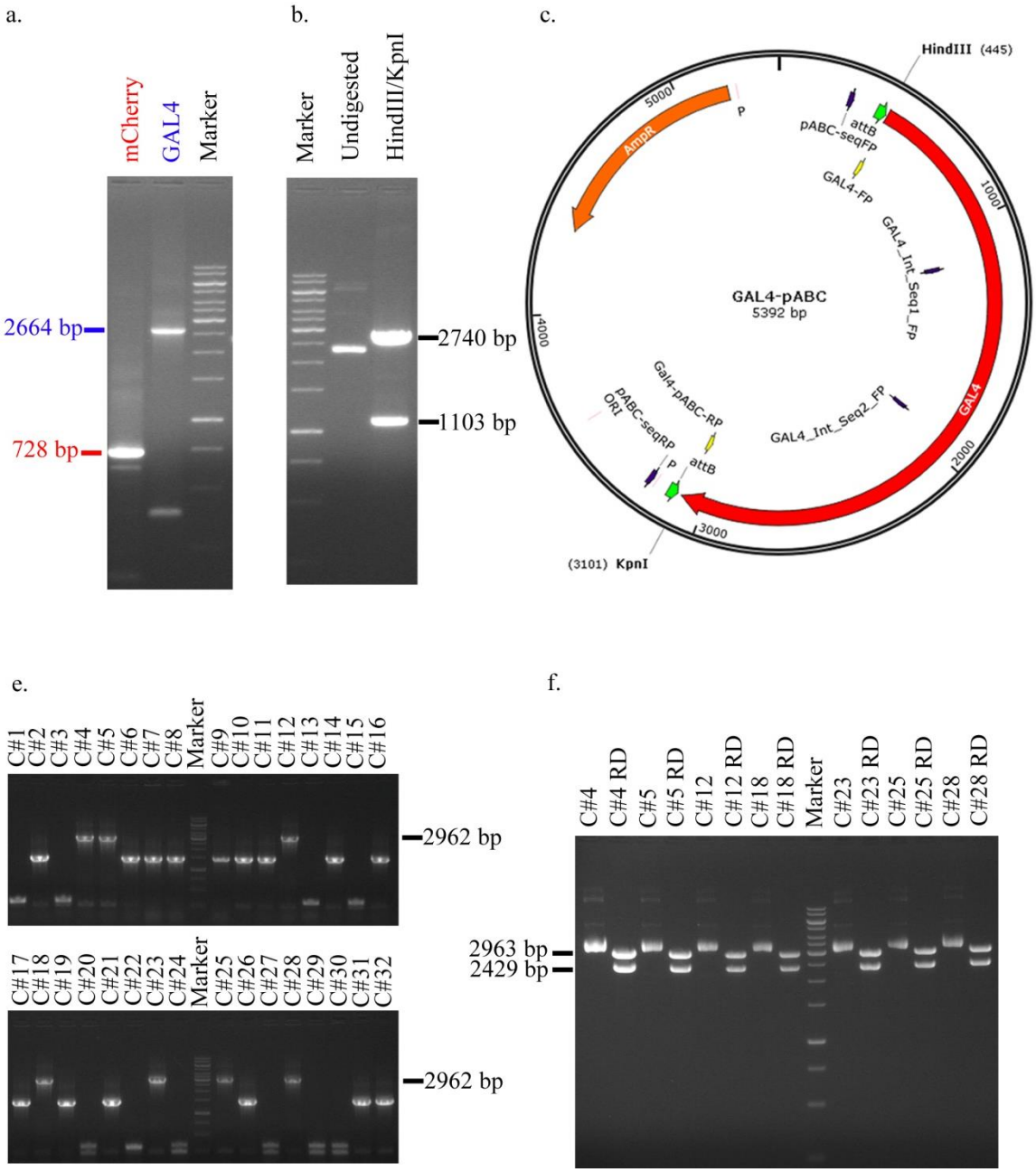

Figure 5.8. Generation of *GAL4*-pABC knock-in construct. (a) High-fidelity PCR, (b) *Hind*III/*Kpn*I digestion of *GDAP1*-pABC, and (c) vector map, (d) colony PCR and (e) analytical digestion with *Kpn*I/*Xho*I of *GAL4*-pABC construct.

After verifying the constructs using Sanger sequencing with pABC and GAL4 sequencing primers (pABC_seq_FP, pABC_seq_RP, GAL4_Int_Seq1_FP and GAL4_Int_Seq2_FP), one of the positive clones was selected for knock-in to *CG4623* knock-out flies in the future.

5.4.2. Generation of Knock-in Construct for *CG4623*-mCherry Reporter

Having the downstream and upstream regulatory elements intact makes it possible to knock-in a reporter gene in place of *CG4623* for analyzing its expression pattern. For this purpose the generation of a *CG4623*-mCherry reporter line was planned and the mCherry-pABC construct was prepared.

After high fidelity PCR for *mCherry* coding sequence with primers that have *Hind*III and *Kpn*I restriction sites (mCherry_ pABC_FP and mCherry_ pABC_RP) for 25 cycles and an annealing temperature 55°C, the product was run on a 1% agarose gel (1X TAE) and the band corresponding to mCherry (728 bp) was purified from the gel (Figure 5.9a). The purified fragment was digested with *Kpn*I and *Hind*III enzymes and purified again without loading on a gel. Using the same enzymes, *GDAP1*-pABC construct was digested to obtain the pABC backbone corresponding to the 2740 bp band on a 1% agarose gel (1X TAE) and it was also purified from the gel (Figure 5.9b). The *Hind*III-mCherry-*Kpn*I fragment was ligated to the pABC backbone digested with the same enzymes.

After transformation, plating on LB agar with ampicillin and overnight growth, colonies were picked for colony PCR, which was done using primers on pABC (pABC_seq_FP and pABC_seq_RP) for 30 cycles with an annealing temperature of 54°C. After running the products on a 1% agarose gel (1X TAE), positive colonies, corresponding to the 1026 bp band, were selected (Figure 5.9c). Isolated plasmids from these positive clones were digested with *Hind*III and *Kpn*I for verification. The restriction digestion products run on a 1% agarose gel (1X TAE) gave the expected pattern of 2740 and 716 bp (Figure 5.9d).

After verifying the constructs using Sanger sequencing with pABC sequencing primers (pABC_seq_FP and pABC_seq_RP), one of the positive clones was selected for knock-in to *CG4623* knock-out flies in the future (5.9e).

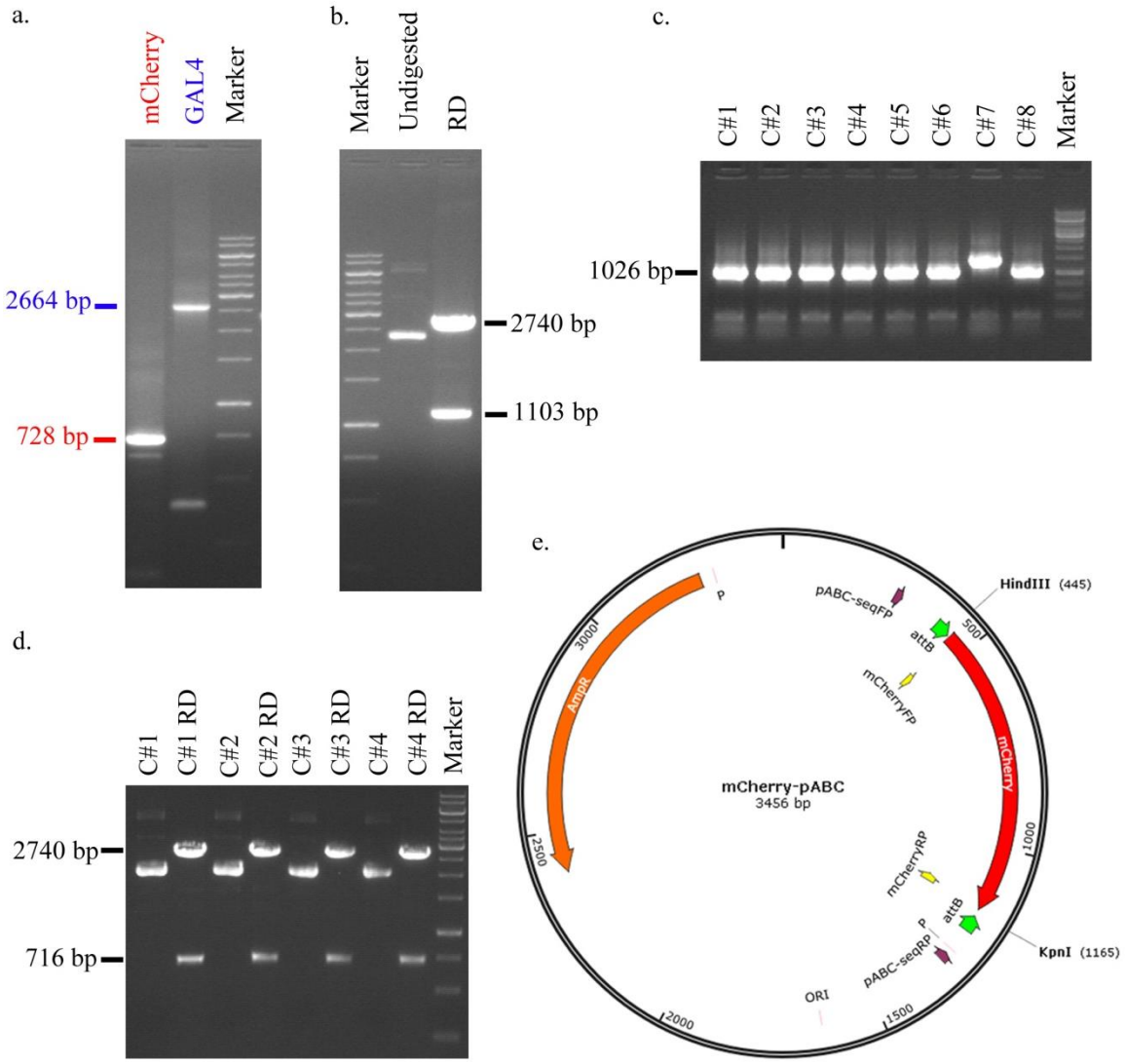

Figure 5.9. Generation of *mCherry*-pABC knock-in construct. (a) High-fidelity PCR, (b) *Hind*III/*Kpn*I digestion of *GDAP1*-pABC, and (c) colony PCR, (d) analytical digestion with *Hind*III/*Kpn*I and (e) vector map of *mCherry*-pABC construct.

5.4.3. Generation of Polyclonal Antibodies Against CG4623

There is no available antibody against CG4623, besides commercially available antibodies against GDAP1 and GDAP1L1 gave low blast scores for the immunogen used to raise these antibodies. This was probably due to the limited identity at the amino acid

level between GDAP1 and CG4623 Thus, it was necessary to produce them at our laboratory.

In order to produce antibodies against CG4623, the first step was the purification of CG4623. For this purpose, *Escherichia coli* was selected as the host and pET30a as the vector, which allows IPTG induced overexpression of a recombinant protein with six histidine residues (His-tag) at the amino or carboxyl terminus. According to the rare codon analysis, by clustering and by number, CG4623 was found to include a relatively high number of rare codons and two clusters (Clarke & Clark, 2008). Therefore, the Rosetta strain (Novagen) was selected as host competent cells as it provides rare codon tRNAs for better expression (Figure 5.10).

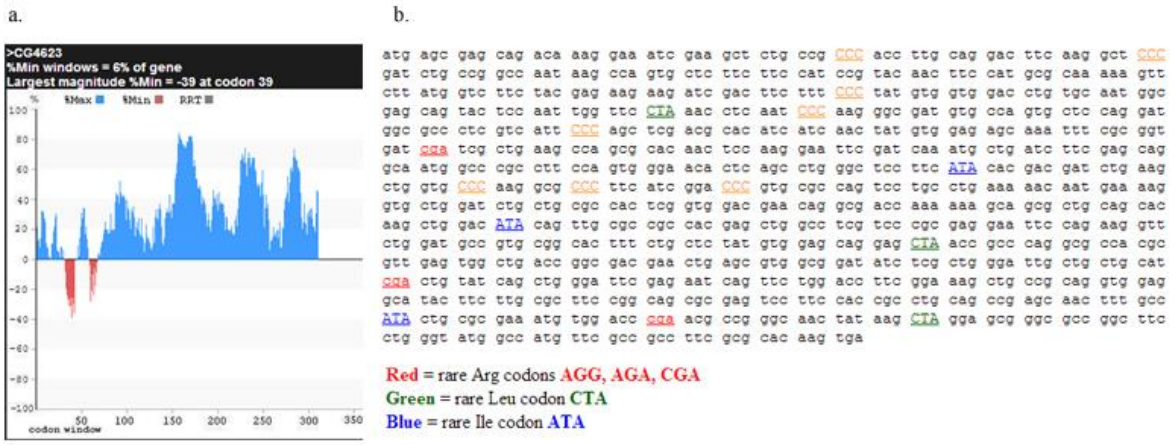

Figure 5.10. Codon bias analysis of CG4623. (a) Rare codon clustering analysis, (b) *CG4623* coding sequence analyzed for five rarest codons in *Escherichia coli* (Clarke & Clark, 2008).

First, *CG4623* cDNA (RE69232) was amplified by high fidelity PCR using primers that had *Kpn*I and *Xho*I restriction sites (CG4623_pET30a_FP and CG4623_pET30a_RP) for 30 cycles at 59°C. The primers were designed to allow the expressed protein to have a His-tag at its N-terminus. After running on 1% agarose gel (1X TAE), the band corresponding to 1000 bp was purified (Figure 5.11a). The fragment was ligated to the pGEM-T Easy vector and after transformation and overnight growth, colonies were picked for colony PCR using T7 and SP6 for 30 cycles at an annealing temperature of 50°C. The

expected band of 1177 bp was observed for all colonies on a 1% agarose gel (1X TAE) (Figure 5.11b).

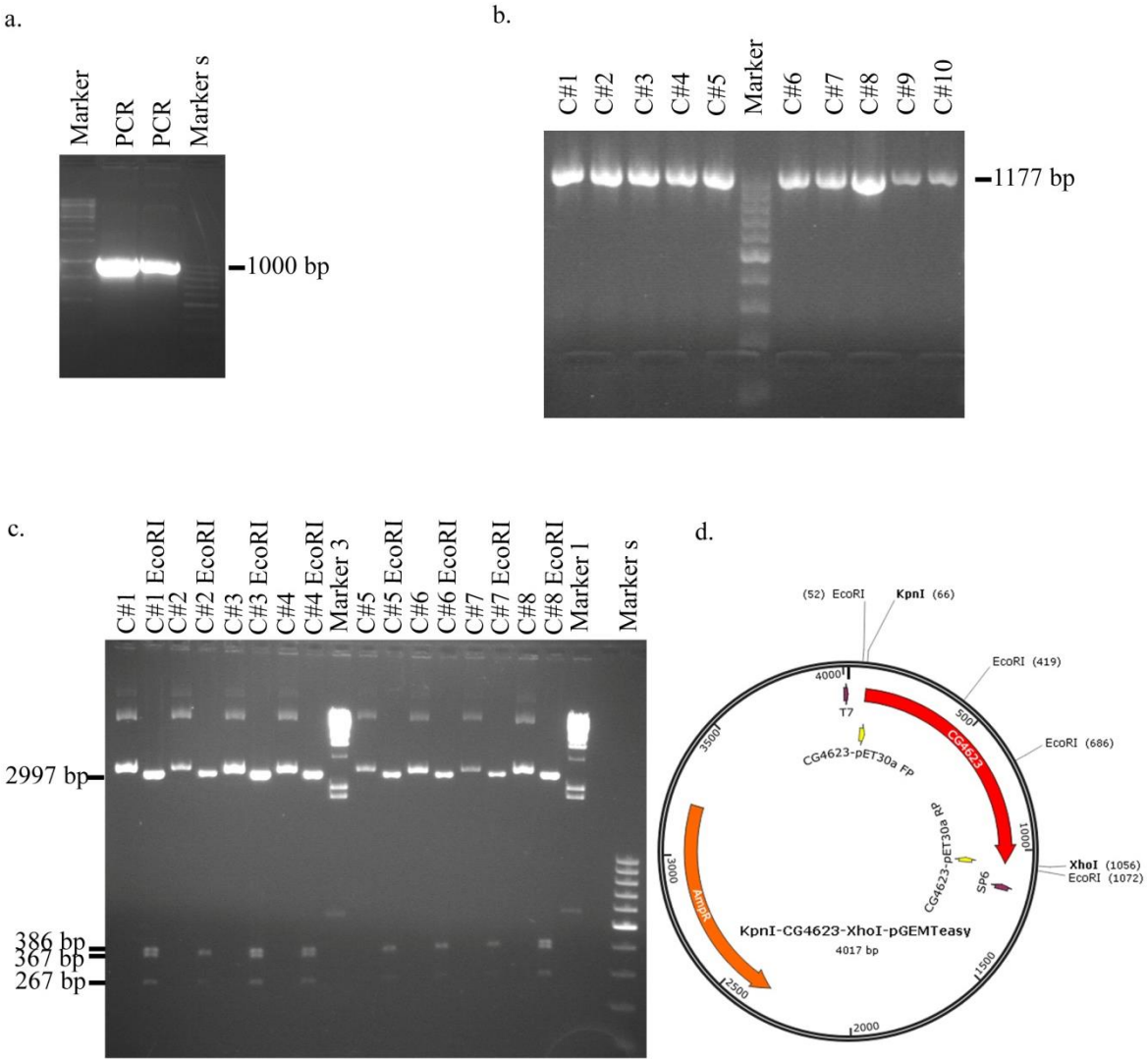

Figure 5.11. Subcloning of *CG4623* for cloning into pET30a. (a) High fidelity PCR, (b) colony PCR, (c) analytical digestion with *Eco*RI and (d) vector map of *Kpn*I-*CG4623*-*Xho*I-pGEM-T Easy construct.

For the selected positive colonies, plasmids were isolated after overnight growth in LB medium with ampicillin and analytical digestion was performed using *Eco*RI. After running the restriction products on a 1% agarose gel (1X TAE), positive colonies giving bands of 2997, 386, 367 and 267 bp according to the vector map were selected (Figure 5.11c-d). Positive colonies were sent to sequencing using T7 and SP6 primers. One of the mutation-free constructs was selected.

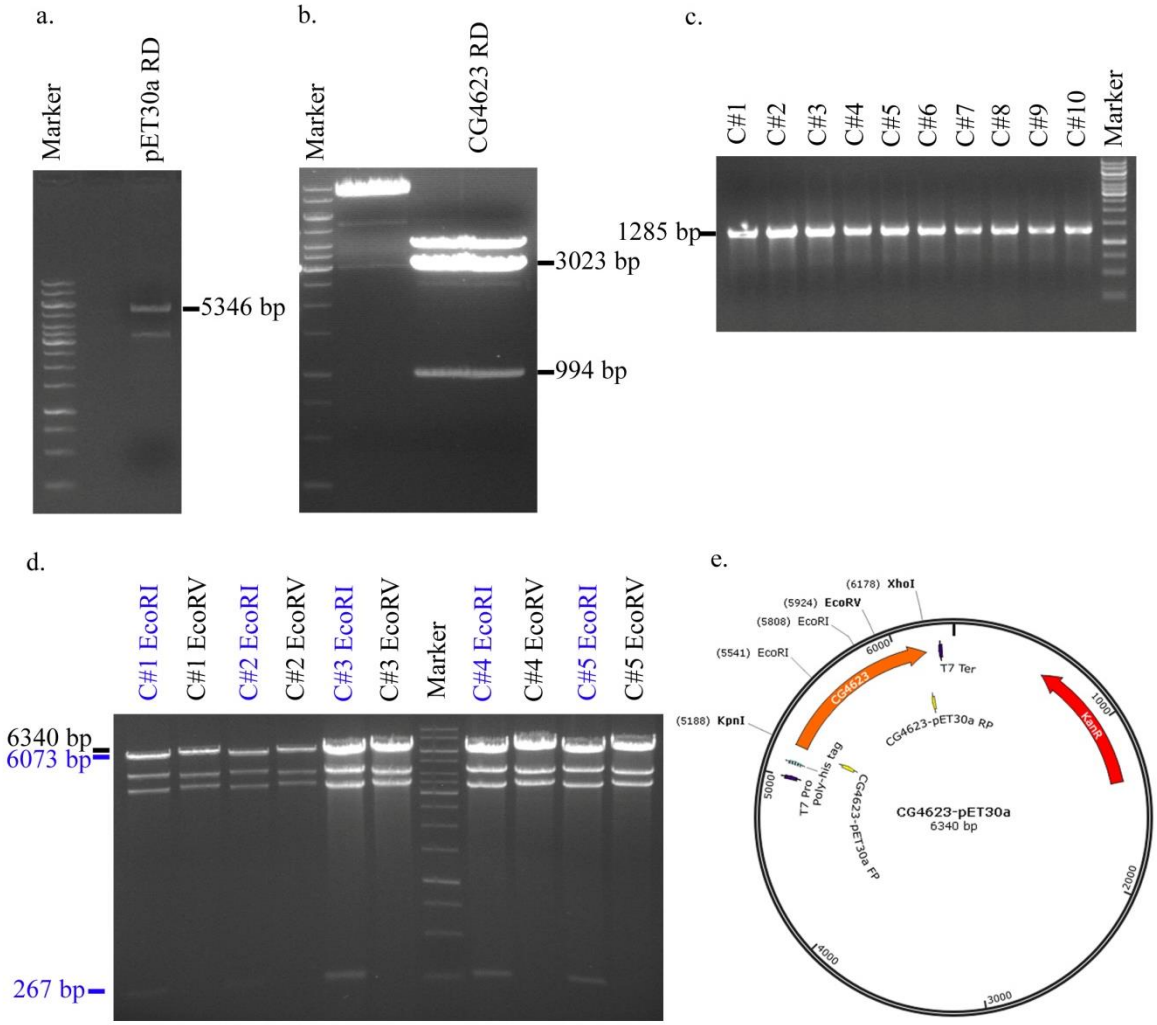

Figure 5.12. Generation of *CG4623*-pET30a construct. *Kpn*I/*Xho*I digestion of (a) pET30a and (b) *Kpn*I-*CG4623*-*Xho*I-pGEM-T Easy, (c) colony PCR, (d) analytical digestion and (e) vector map of *CG4623*-pET30a construct

In order to clone *CG4623* into pET30a, both pET30a and *Kpn*I-*CG4623*-*Xho*I-pGEM-T Easy were digested with *Kpn*I and *Xho*I. After running the products on a 1% agarose gel (1X TAE), the fragments corresponding to the pET30a backbone (5346 bp) and *CG4623* (994 bp) were purified from the gel (Figure 5.12a-b). They were ligated to each other and the ligation product was used to transform the competent Rosetta cells. Colony PCR was done using T7 and T7 terminator universal primers that lie on the pET30a backbone. Positive colonies corresponding to 1285 bp were selected for growth in LB medium with kanamycin (for pET30a) and chloramphenicol (for Rosetta's rare codon plasmid), and plasmids were isolated (5.12c). Using *Eco*RI and *Eco*RV, analytical digestions were done. After running the products on a 1% agarose gel (1X TAE), 6073 and

267 bp bands were observed for *EcoR*I and a band of 6340 bp was observed for *EcoR*V digestion as expected (Figure 5.12d). The prepared constructs were sent to Sanger sequencing with T7 and T7 terminator primers (Figure 5.12e). A mutation-free clone was selected and glycerol stock for this overexpression strain was obtained.

Initial purification efforts failed even though overexpression was observed and his-tagged protein was detected in Western blots using anti-His antibody. The formation of dimers and thus insoluble form of CG4623 *in vitro* might have caused the difficulties. Currently, using this overexpression strain, CG4623 is being overexpressed and purified by nickel columns for injection into animals for immunogenic response. When CG4623 is purified, cross-reactivity test using GDAP1 and GDAP1L1 antibodies that were raised with the closest-resembling immunogen are planned.

5.5. Analysis of Fly Lines with Mitochondrial Dynamics-Related Deficiencies

In order to understand the effect of high levels of *CG4623*, we planned to analyze the UAS-*CG4623* overexpression line in terms of longevity, motor performance, mitochondrial dynamics and oxidative stress along with immunohistochemical staining and electrophysiology. Therefore, two fly genes involved in mitochondrial dynamics *Drp1* (homolog of human *Drp1*) and *Marf* (homolog of human *Mfn1* and *Mfn2*) were taken as a model. Homozygous lethal deficiency lines that have large chromosomal deletions including these genes were obtained along with a loss of function mutant form of *Drp1* to be analyzed in terms of longevity. RNAi lines for these two genes were also obtained and analyzed in terms of mitochondrial dynamics.

5.5.1. Longevity Assay

After following female and male flies over 64 days by counting the number of dead flies during every two or three days, the longevity curves were drawn and statistically analyzed for *Drp1* deficiency, $Drp1^{T26}$ loss of function line, *Marf* deficiency line and w^{1118} line as control using online using an online tool (Yang *et al*., 2011).

The survival graphs for males and females over 64 days were drawn (Figures 5.13 and 5.14, respectively). *Marf* deficiency line, which includes various genes deleted along with *Marf* on the X chromosome, yielded lower survival percentages over the documented period.

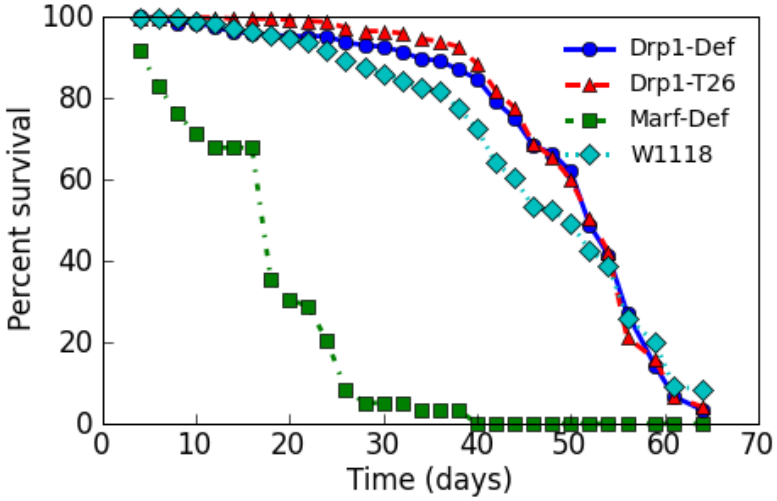

Figure 5.13. Survival graph for males of four fly lines. Drp1-Def, Drp1-T26, Marf-Def, W1118 stand for male flies with *Drp1* deficiency, $Drp1^{T26}$ loss of function mutant, *Marf* deficiency and w^{1118} control line, respectively (Yang *et al*., 2011).

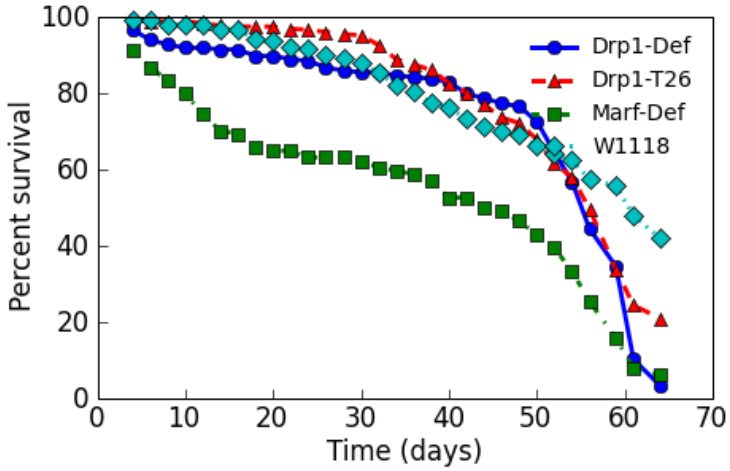

Figure 5.14. Survival graph for females of four fly lines. Drp1-Def, Drp1-T26, Marf-Def, W1118 stand for female flies with *Drp1* deficiency, $Drp1^{T26}$ loss of function mutant, *Marf* deficiency and w^{1118} control line, respectively (Yang *et al*., 2011).

In both of the graphs, males had lower percent survival over time compared to females. *Drp1* lines yielded similar phenotypes compared to control in males; however, in

females, the number of flies alive decreased rapidly around 60 days for *Drp1* mutant female flies compared to the control. Detailed analysis of survival in terms of mean lifespan and age in mortality percentage can found in Tables 5.3 and 5.4 for males and females, respectively.

Table 5.3. Detailed longevity analysis for males of four lines (Yang *et al*., 2011).

Line	**Number of Subjects**	**Restricted mean**			**Age in days at % mortality**				
		Days	Std. error	95% C.I.	25%	50%	75%	90%	95% Median C.I.
Drp1-Def	268	49.88	0.73	48.45 ~ 51.32	46	52	59	61	52 ~ 52
Drp1-T26	362	51.06	0.48	50.11 ~ 52.00	46	54	56	61	52 ~ 52
Marf-Def	59	17.49	1.13	15.28 ~ 19.70	10	18	24	26	- ~ -
W1118	342	47.18	0.73	45.75 ~ 48.61	40	50	59	61	46 ~ 50

Table 5.4. Detailed longevity analysis for females of four lines (Yang *et al*., 2011).

Line	**Number of Subjects**	**Restricted mean**			**Age in days at % mortality**				
		Days	Std. error	95% C.I.	25%	50%	75%	90%	95% Median C.I.
Drp1-Def	234	50.18	1.09	48.05 ~ 52.31	50	56	61	64	56 ~ 56
Drp1-T26	352	52.75	0.66	51.46 ~ 54.05	46	56	61	-	56 ~ 56
Marf-Def	114	37.42	2.07	33.37 ~ 41.47	12	46	59	61	36 ~ 50
W1118	319	52.31	0.89	50.57 ~ 54.04	42	61	-	-	61 ~ 61

According to detailed longevity analysis for males, *Marf* mutants lived shorter than average even though the vials were changed every two or three days renewing food and limiting contamination of all types. *Drp1* mutants and w^{1118} control flies had similar lifespan for the majority of the assay. Even though w^{1118} control lines were mite infected and therefore had flies of smaller size and probably worse health, the longevity statistics show that there is a significant difference in longevity between *Marf* deficiency line and

other lines. *Drp1* mutations were found not to be affecting longevity compared to controls. The results of the Fisher's exact test for each combination of genotypes could be found in Table 5.4.

Table. 5.5. Fisher's exact test results for females (Yang *et al*., 2011).

Condition	**Statistics**			
	P-value at 25%	P-value at 50%	P-value at 75%	P-value at 90%
Drp1-Def vs. Drp1-T26	0.68600	0.23720	0.85910	0.00001
Drp1-Def vs. Marf-Def	<0.00001	0.00004	0.56180	0.56180
Drp1-Def vs. W1118	0.06780	0.21860	<0.00001	<0.00001
Drp1-T26 vs. Drp1-Def	0.68600	0.23720	0.85910	0.00001
Drp1-T26 vs. Marf-Def	<0.00001	0.00010	0.00020	0.00010
Drp1-T26 vs. W1118	0.00470	0.52230	<0.00001	<0.00001
Marf-Def vs. Drp1-Def	<0.00001	0.00004	0.56180	0.56180
Marf-Def vs. Drp1-T26	<0.00001	0.00010	0.00020	0.00010
Marf-Def vs. W1118	<0.00001	0.00010	<0.00001	<0.00001
W1118 vs. Drp1-Def	0.06780	0.21860	<0.00001	<0.00001
W1118 vs. Drp1-T26	0.00470	0.52230	<0.00001	<0.00001
W1118 vs. Marf-Def	<0.00001	0.00010	<0.00001	<0.00001

5.5.2. Mitochondrial Network Dynamics Analysis

Drp1 and *Marf* RNAi lines were crossed to motorn neuron driver D42-GAL4. The progeny included flies expressing dsRNA targeting either *Drp1* or *Marf* in motor neurons, where GFP with mitochondrial import signal was also produced. The ventral nerve cord and brain of the third instar larvae were dissected and motor and sensory neuron bundless projecting from the nerve cord were analyzed at a magnification of 20X with no digital zoom by taking the maximum projections of all stacks of 1.5 μm thickness (Figure 5.15). *Marf* downregulation compared to *Drp1* downregulation may have caused more spherical mitochondria as tubular structures are missing.

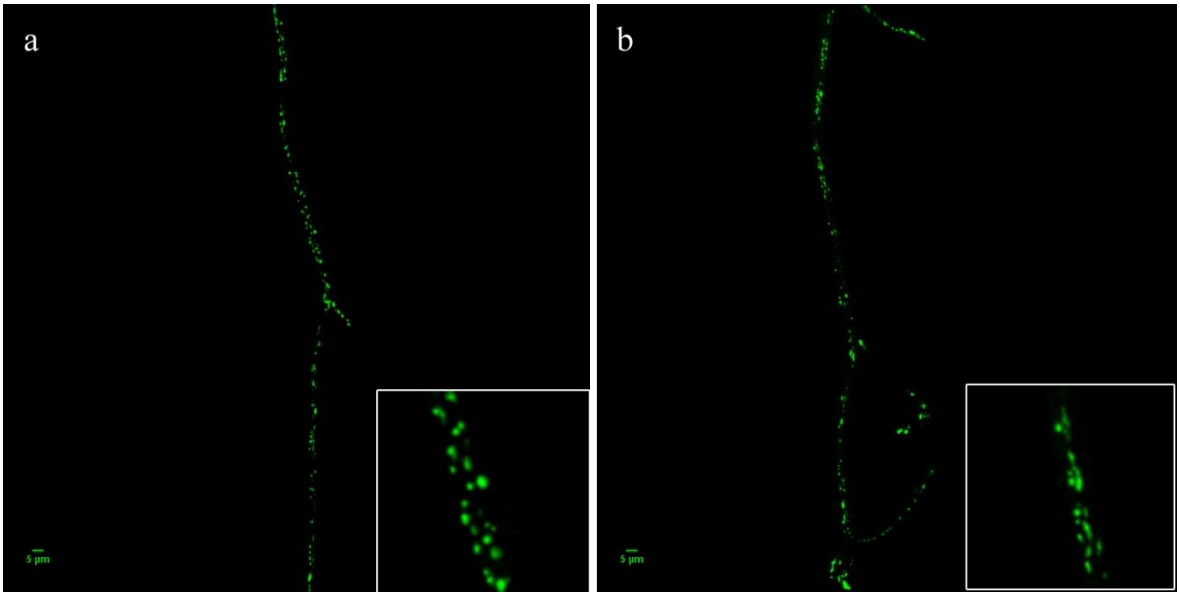

Figure 5.15. Mitochondria in motor neuron bundles of *Marf* and *Drp1* downregulated flies after ventral nerve cord dissection. (a) *Marf* downregulation, (b) *Drp1* downregulation and GFP signal tags mitochondria.

Neuromuscular system of the third instar larvae was also dissected and motor and sensory neuron bundles were again analyzed this time at a magnification of 63X with 0.59 µm thickness by taking the maximum projections (Figure 5.16).

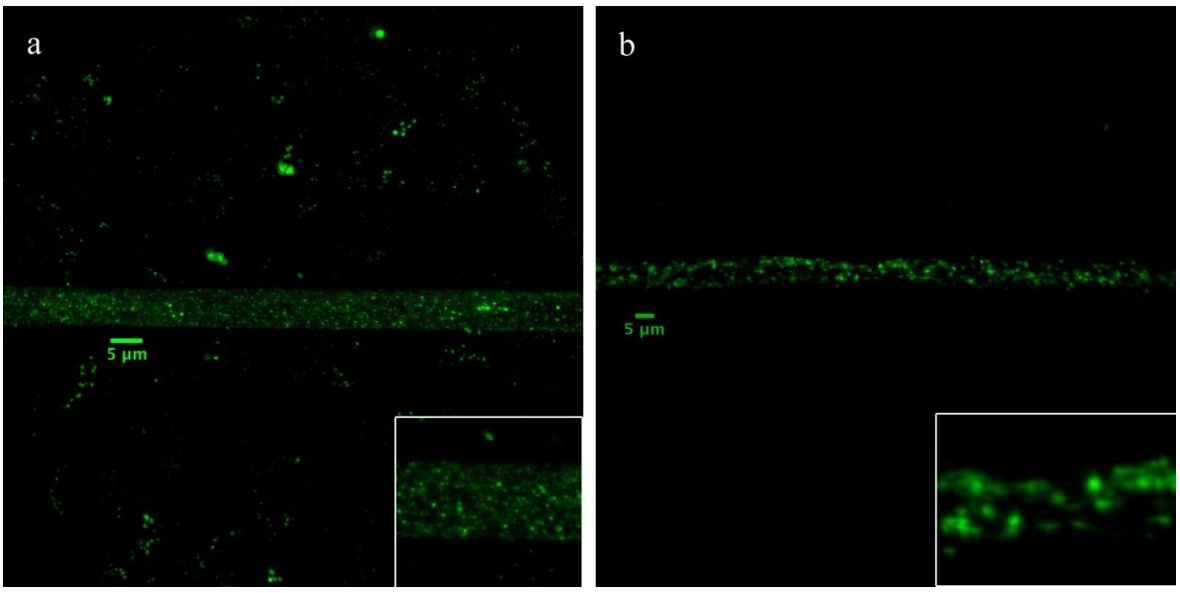

Figure 5.16. Mitochondria in motor neuron bundles of *Marf* and *Drp1* downregulated flies after neuromuscular system dissection. (a) *Marf* downregulation (2.7 digital zoom), (b) *Drp1* downregulation and GFP signal tags mitochondria.

When the neuromuscular system was analyzed in terms of mitochondrial morphology, it was observed that downregulation of mitochondrial fusion factor *Marf* caused formation speck-like structures, rather than tubular mitochondria (Figure5.16), compared to the more tubular structures observed in downregulation of the fission factor *Drp1*.

5.5.3. Eclosion Assay

In order to assess whether downregulation of *Marf* or *Drp1* affects the number of flies emerging from pupae, a preliminary eclosion assay was performed. This was done by crossing ubiquitous driver (act5c-GAL4) to the RNAi lines (UAS-Marf-RNAi or UAS-Drp1-RNAi). The emerging flies were counted according to their genotypes by checking their sex and markers by visual inspection. The resulting phenotypes could be observed in Table 5.5. However, due to small size, the data was not reliable. Chi-square test yielded a p-value of 0.08 and 0.78 for *Marf* and *Drp1* compared to the control, respectively.

Table 5.6. Eclosion assay results for *Marf* and *Drp1* ubiquitous downregulation and the control. Each cell contains the number of progeny according to RNAi activation by the presence of act5c-GAL4 driver and sex in two crosses.

Drp1	**C#1 ♂**	**C#1 ♀**	**C#2 ♂**	**C#2 ♀**
RNAi active	26	36	28	26
RNAi inactive	30	34	24	31
Marf	**C#1 ♂**	**C#1 ♀**	**C#2 ♂**	**C#2 ♀**
RNAi active	8	22	2	4
RNAi inactive	16	21	2	4
Control	**C#1 ♂**	**C#1 ♀**	**C#2 ♂**	**C#2 ♀**
y,v; act5c-GAL4/+	31	24	25	31
y,v; Cyo, roi/+	30	36	28	20

5. DISCUSSION

In this study, I have focused on three major aspects of developing *Drosophila* model for Charcot Marie Tooth disease: generation of tools for integrase-mediated approach for gene knock-out, generation of the *CG4623* overexpression line and analysis of available mutants for genes that are involved mitochondrial dynamics.

In the first part of the study, there were two major goals to be accomplished: generation of tools for showing functional homology between *CG4623* and *GDAP1* and those for modeling the disease. In order to show that *CG4623* and *GDAP1* are functional homologs, the phenotype that is expected to be observed when *CG4623* is knocked-out must be rescued by *GDAP1* knock-in. Therefore, a construct for knocking-in *GDAP1* using *ΦC31* integrase mediated transgenesis was generated. Using this construct, it will be possible to eventually replace *CG4623* (rather the marker gene that should be in place of *CG4623*) with *GDAP1* without disturbing any neighboring sequences. It should be noted that upstream and downstream regions of the gene are planned to be kept intact as these regions are thought to be harboring regulatory elements that determine expression pattern and level of *CG4623*. Ideally, it is expected that by knocking-in *GDAP1*, the expression levels and pattern of this gene will match that of *CG4623*; however, it is also possible that on *CG4623* itself, for instance, in one of the introns, a regulatory element could reside. Therefore, knocked-in *GDAP1* levels and pattern should be characterized when this line is generated.

The available information regarding *CG4623* on databases showed that the expression levels were low. However, in our unpublished quantitative RT-PCR analysis, we have observed that *CG4623* is expressed at approximately 6.25% of *Actin79b* in a mixed population of flies of both sexes according to total RNA isolation from head of five week old flies. Therefore, it is vital to expand current knowledge on expression levels and pattern of this gene in order to compare its function to *GDAP1*, which is expressed predominantly in the peripheral nervous system. For this purpose, two different knock-in constructs were generated. The first one is the *CG4623*-GAL4 construct, which will allow generation of a GAL4 driver for *CG4623* by replacement of this gene with GAL4 coding

sequence. Using this driver, it will be possible to express a specific reporter such as GFP to approximate expression pattern and to some extent level of *CG4623*. In this case GAL4 is produced possibly at a level compared to CG4623; however, it will cause overexpression by binding to a UAS responder element as it is a transcription factor; therefore this would not be the right technique to approximate expression levels. Considering this drawback, a knock-in construct that had mCherry coding sequence was also prepared. The difference between expressing mCherry by replacing *CG4623* and expressing mCherry by crossing *CG4623*-GAL4 line to UAS-mCherry will be evident in the difference between the expression levels even though pattern will be similar. Using mCherry knock-in line, we may be able to observe a similar pattern and level of expression compared to *CG4623*. However, a major advantage of *CG4623*-GAL4 line would be to overexpress a specific gene for which UAS responder line is available without knocking it in, such as other proteins involved in mitochondrial dynamics. This way, we may understand whether, the loss of *CG4623* could be rescued by overexpressing another fission factor, such as *Drp1*, or by overexpressing RNAi targeting a fusion factor, such as *Marf*.

In case that it takes time to knock-out *CG4623* and knock-in different constructs using IMAGO, it is possible to understand expression pattern using bacterial artificial chromosome (BAC) recombineering approach (Warming, Costantino, Court, Jenkins, & Copeland, 2005). In this method, a *Drosophila* genomic library BAC that includes *CG4623* and large flanking regions is obtained. Selecting short homology arms just before the stop codon, a *galK* coding sequence is PCR amplified and transformed into cells that have precise deletions for this gene. Using homologous recombination machinery, the PCR product may recombine to the 3' end of CG4623. Therefore the recombinants can be selected using minimal media that has galactose as the only carbon source as these bacteria have *galK* deleted. Then a reporter such as GFP is PCR amplified using the same homology arms and transformed into these cells. The cells that have gone through homologous recombination and that had *galK* replaced by the reporter gene will survive in the presence of 2-deoxy-galactose, which yields a toxic byproduct when used as a substrate by galK. At the end, a BAC that includes a fusion protein of CG4623 and a reporter gene, such as GFP, is obtained. This way, the generated fly line by microinjection of this construct will be able to produce an extra copy of CG4623 with a GFP tag.

Analysis of CG4623 expression levels and pattern would best be determined by western blot and immunohistochemistry using anti-CG4623 antibody; however, as there is no available antibody against this protein, our aim was to produce it. For this reason, the initial step was to overexpress our protein of interest in bacteria. We already knew that it was not easy to produce GDAP1 in large amounts in bacteria due to its transmembrane domain, which resulted in dimerization of the protein and made it insoluble. There weren't any reports regarding purification of CG4623, therefore we firstly analyzed the codon bias of this protein and dimerization potential, and realized that the high number of rare codons would make it difficult to produce in any bacterial cell. Therefore we opted for a bacterial strain that includes a plasmid that codes for rare codon tRNAs. Initial experiments showed that the protein can be overexpressed, which we detected by SDS-PAGE by size and western blot with anti-His antibody. As I didn't have success with commercially available Ni-NTA spin columns, currently the purification is being done by colleagues using a nickel column and various chemical treatments.

Besides generation of constructs for knocking mCherry and GAL4 sequences in place of *CG4623*, constructs for *GDAP1* and mutant versions of *GDAP1* knock-in were also generated. Using *GDAP1* knock-in line, it will be possible to validate the functional homology to *CG4623*, by assessing the changes in the phenotype. Our *a priori* assumption is that homozygous loss of *CG4623* would generate a phenotype related to the nervous system. Considering that *GDAP1* is expressed predominantly in the peripheral nervous system while its paralog *GDAP1L1* is expressed in the central nervous system, it is possible that *CG4623*, which has approximately equal similarity to both genes, could have an important function in both parts of the nervous system. Therefore, in the analysis of the phenotypes using behavioral assays, the focus should not only be on motor and sensory involvement, but also possible defects in the central nervous system, such as learning and memory.

After analysis of the homozygous loss of *CG4623* using knock-out flies that are being generated, *GDAP1* knock-in construct prepared in this study should be used to determine the extent of rescue in terms of the phenotypes observed. However, rather than complete loss of *CG4623*, the effect of mutant versions of *GDAP1* in terms of generating a phenotype should be assessed. Nine missense mutations that differ in terms of their

characteristics have been chosen to be modeled. Among these, there are mutations that are dominantly (R120W, T157P, C240Y) and recessively (P78L, R120Q, D149Y, P153L, G271R, Y279C) inherited including a compound heterozygosity case that causes a severe phenotype (R120W and G271R). Similarly, mutations were also selected to model axonal (R120W, T157P, C240Y, G271R, Y279C), demyelinating (R120Q) and intermediate (P78L, D149Y, P153L) phenotypes. As *Drosophila* does not have a proper myelin structure and *GDAP1* mutations mostly cause axonal or intermediate subtypes, most of the mutations were chosen from these two. However, considering that the glia wrap around the axons in a similar manner to myelin sheath, loss or increase of this structure should be analyzed in these mutants.

Due to the limited identity at the amino acid level, only six of the missense mutations are on residues that are conserved in *Drosophila*, therefore care has been taken to select four of these conserved sites to model mutations (P78L, P153L, G271R, Y279C). It was also important to choose mutations according to domains that they are located on: GST-N (P78L), α4-α5 loop (P153L, T157P) and GST-C (C240Y, G271R, Y279C). Lastly mutations were selected according to the onset and severity of the disease phenotype. Since the *Drosophila* life cycle is short, it is possible that the effects of late-onset mutations could not be observed or early-onset mutations with severe phenotype could be lethal. Therefore, some of the mutations chosen to be modeled had severe disease phenotypes with early onset (P78L, P153L, T157P, Y279C) while some had milder progression.

Although more than half of the *GDAP1* mutations are missense, there are also frameshift, nonsense and splicing mutations; however, only nine missense mutations were chosen to be modeled. This is due to the fact that by knocking out *CG4623*, we have the chance to observe the possible effect of many of the mutations that cause the disease through a complete loss of function mechanism, such as early truncated forms of the protein. Furthermore, by modeling through a single residue changes, it is planned to pin down the pathogenic mechanism to a certain function as well as finding a common mechanism or modifier that could shed light on the CMT disease in general.

Due to differences between mammalians and insects, it is possible that some of these mutations to be modeled would not yield any recognizable phenotype in the nervous

system. This is the rationale behind our strategy of choosing integrase-mediated approach for gene knock-out, as it is easier to knock-in a mutant version of a gene using recombinase mediated cassette exchange. Therefore, generation of nine transgenic flies carrying different mutant forms of *GDAP1* will allow us to select for observable phenotypes and continue analyses of these rather than trying to model a single mutation, which may or may not yield a phenotype at all. When the *GDAP1*-mutant flies are generated, they should be initially analyzed in terms of their motor and sensory performance using behavioral assays. Initially, the focus should be on those that exhibit the strongest resemblance in terms of disease phenotype to human peripheral neuropathy. This way, it will be more feasible and time-saving to understand CMT pathogenesis in flies.

The second part of the study focused on generation of a UAS-*CG4623* responder line. This newly generated fly line, has a *CG4623* coding sequence with UAS element in its upstream, integrated into the short arm of the third chromosome (3L) at the attP2 site (68A4). By crossing this line to a driver such as act5c-GAL4, elav-GAL4, repo-GAL4, OK6-GAL4/D42-GAL4 and mhc-GAL4, it will be possible to observe effects of overexpressing *CG4623* ubiquitously, in all neurons, glia, motor neurons and muscles, respectively. By analyzing the effects of overexpression in the phenotype, it will be possible to shed light on the function of this gene by comparing the phenotype to both wildtype and *CG4623*-downregulated flies using RNAi.

As the UAS-*CG4623* flies have been generated only recently, we haven't had the chance to analyze the expression levels. However, this can be done by isolating RNA from the heads of male and female flies after crossing the overexpression line to the ubiquitous driver (act5c-GAL4). As we have received, three different independent lines after injection and these could have differing expression levels depending on the direction of the landing of our construct. Therefore, these lines have to be crossed separately in order to find the most effective and the least effective overexpression line. Then, all of the three lines could be used to drive the expression, depending on the necessary overexpression level.

Although the quantitative RT-PCR primers, were selected to be on neighboring exons with a large intron in between, it would not have been possible to prevent DNA-contamination in amplification except for DNAse I treatment for overexpression lines. This

is merely due to the fact that overexpression construct includes the cDNA of *CG4623*, therefore genomic DNA harboring this construct would serve as a template if it were not degraded by DNAse treatment.

Due to the fact that UAS-*CG4623* flies are balanced using TM3 chromosome, they do not have a marker selectable during larval stages. Therefore, it has not been possible to select for larvae that carry UAS-*CG4623* and GAL4 driver in order to do dissection and immunohistochemistry at the larval stages. In order overcome this problem it is either possible to balance UAS-*CG4623* with a balancer such as TM6B, which has a larval marker, or recombine UAS-*CG4623* with UAS-mitoGFP, which will allow tracking of this trait using signal from GFP carrying mitochondrial import signal. The latter is much feasible, as by doing this, analysis of mitochondrial dynamics will be possible with a single cross to a driver such as act5c-GAL4 or OK6-GAL4, for ubiquitous or motor neuron expression.

Another use of UAS-*CG4623* is to validate the knock-out line by rescuing the possible phenotype to be observed. By overexpressing *CG4623*, spatiotemporally in flies that have homozygous deletions of this gene, it will be possible to delineate the developmental stage and tissues, in which the expression of this gene is vital for rescue of the phenotype. This way, it is possible to shed light on the role of *CG4623* by analyzing its importance time- and tissue-wise.

In the third part of this study, available mutant lines for mitochondrial dynamics related genes were analyzed in terms of mitochondrial dynamics and longevity. These lines were *Marf*-deficieny, deletion of a chromosomal region that includes CMT-causing mitochondrial fusion factors *Mfn1*/*Mfn2*'s homolog and *Drp1*-deficiency, deletion of a chromosomal region that includes mitochondrial fission factor *Drp1*'s homolog along with $Drp1^{T26}$, the loss of function mutant form of *Drp1*. Although larval neuromuscular system was dissected as well as brain and ventral cord in order to analyze mitochondrial dynamics, it was not possible to quantify the observed differences among phenotypes due to lack of image analysis tools to quantify mitochondrial dynamics parameters reliably. However, between *Drp1*–RNAi and *Marf*–RNAi, there was a morphological difference in line with what is expected, where there were more tubular mitochondria in *Drp1*–RNAi and speck-

like mitochondria in *Marf*–RNAi. Since *Marf* is a mitochondrial fusion factor, its downregulation may result in smaller, spherical mitochondria while downregulation of *Drp1* is expected to yield more mitochondria that are elongated.

In terms of longevity, *Marf*-deficiency line had significantly lower lifespan compared to both control (*w1118*) and *Drp1* mutants. There wasn't statistically significant difference in comparisons among control and *Drp1* mutants initially; however, the difference increased over time, especially in females. This finding is supportive of our choice of *Drosophila* as a model organism since *Mfn1* and *Mfn2* mutations are one of the major causes of CMT, whereas mutations in *Drp1* have not yet been linked to peripheral neuropathy. It is apparent that the CMT-associated gene has a vital conserved function, which may be the case for *CG4623,* too.

In the longevity assay, it was observed that the flies had limited capacity of movement during the late phases of the study. It was also noted that some of the mutants were more prone to the effects of static electricity, possibly due to their curly wings. Therefore, in future studies, removal of balancer chromosomes should be a high priority before starting the assay. This way, side effects from these secondary characteristics will be eliminated. Even though compared to the wildtype (w1118), *Drp1* mutants had similar longevity curves over a long duration, this was possibly due to the fact that control flies already had mite contamination. As mite contamination causes flies to be smaller in size during eclosion and possibly with poor health, this could have an effect in the results of the assay. Therefore, mite contamination should be eliminated at least one generation before the assay's beginning.

Besides mutants for *Marf* and *Drp1*, RNAi lines of these genes were also analyzed in terms of their developmental capacity using eclosion assay. In this assay, by crossing ubiquitous driver with the RNAi lines, it was aimed to study the number flies that have the genotype that caused downregulation (act5c-GAL4 and UAS-RNAi for *Marf* or *Drp1*) compared to the genotype that did not have downregulation (flies that did not carry GAL4 driver and UAS responder in their genotype). In this preliminary assay, due to small size, it was not possible to draw statistically significant conclusions.

The longevity and eclosion assays were performed in order to form the basis to assess the function of *CG4623* and its loss' effect on the organism, in the future. Therefore, the available *CG4623* deficiency line (approximately 20 genes are deleted in this chromosomal aberration), downregulation and overexpression lines of *CG4623* should be compared in terms of longevity and eclosion to wildtype. When the precise knock-out is obtained using IMAGO, it should also be included in these assays in order to analyze its effect compared to the other lines studied.

Lastly, in order to generate an imprecise excision allele of *CG4623*, *Minos* transposable element in the intronic region of the gene was tried to be mobilized. For this purpose a *Minos* carrying line was crossed with a *Minos* transposase carrying line. After obtaining mosaic eyed flies, showing that *Minos* element was indeed mobilized, the balanced progeny of these mosaic flies were analyzed in terms of possible deletion of a neighboring sequence. For this purpose, genomic PCR was employed using primers that were at least 1.3 kb away from the position of the *Minos* element.

Out of 76 generated *Minos*-deletion lines, none of them carried an imprecise deletion according to our analysis. However, it should be noted that with our methodology, it was not possible to find any deletion that caused the loss of a region where the primers bind. In other words, any deletion beyond the 1.3 kb distance from the transposable element would have caused a false negative using the current primers. Furthermore 76 lines may not have been enough to observe imprecise excision. Therefore, the number of lines analyzed should be increased further and, the primer binding sites for screening PCR should be moved further away from the transposable element in order not to miss deletions of larger sizes.

In this study, we have generated tools to model Charcot-Marie-Tooth disease, with a focus on subtype CMT4A, using integrase-mediated approach for gene knock-out and by overexpression. Using available mutants, we have analyzed longevity and mitochondrial dynamics. The future study may focus on using the available tools in analyzing the flies that have been and will be generated. However, it should also be noted that the toolkit should be extended by assessing motor and sensory performance with larval crawling, negative geotaxis and sensory assays, oxidative stress levels, *in vivo* live imaging of mitochondrial dynamics, morphological analysis of nervous tissues and functional analysis

using electrophysiology. This way, it will be possible to recapitulate motor and sensory neuropathy in flies.

6. CONCLUSION

In this study, major steps of establishing the *Drosophila* CMT model have been taken. The construct generated for knocking-in human wildtype gene in place of its *Drosophila* homolog will allow understanding whether *GDAP1* and *CG4623* are functional homologs. The major reason for choosing integrase-mediated approach for gene knock-out was to be able to knock-in numerous constructs easily and site-specifically using bacterial and phage attachment sites, *attB* and *attP*, via recombinase mediated cassette exchange. Therefore, nine mutant forms of *GDAP1* were generated using site-directed mutagenesis and these constructs are ready for injection. With analysis of these fly lines to be generated, it will be possible to delineate the mechanism through which these mutations cause the pathogenesis of CMT. The mutations to be modeled were selected from a wide range as it is possible that some of them would not yield a phenotype in *Drosophila*. Therefore, mutations, which are on different domains causing axonal, demyelinating or intermediate subtypes with dominant or recessive segregation, mild/late onset and severe/early onset phenotypes, have been chosen to be modeled, with focus on those that are conserved in *Drosophila*. In the second part of this project, a UAS responder line for *CG4623* (UAS-*CG4623*) has been generated in order to study the function of this gene through overexpressing it spatio-temporally and comparing it to RNAi line and the wildtype flies. In the last part of this study, longevity and mitochondrial dynamics analyses have been used to study available mutant and downregulation lines of mitochondrial dynamics related genes, *Drp1* and *Marf*. These assays may be used to analyze the overexpression line generated in this study as well as those lines to be established by injection of the generated constructs.

REFERENCES

Altschul, S. F., T. L. Madden, A. A. Schaffer, J. Zhang, Z. Zhang, W. Miller and D. J. Lipman, 1997, "Gapped BLAST and PSI-BLAST: A New Generation of Protein Database Search Programs", *Nucleic Acids Research*, Vol. 25, No. 17, pp. 3389-3402.

Altschul, S. F., J. C. Wootton, E. M. Gertz, R. Agarwala, A. Morgulis, A. A. Schaffer and Y. K, Yu, 2005, "Protein Database Searches Using Compositionally Adjusted Substitution Matrices", *Federation of European Biochemical Societies Journal*, Vol. 272, No. 20, pp. 5101-5109.

Ammar, N., E. Nelis, L. Merlini, N. Barisic, R. Amouri, C. Ceuterick, J. J. Martin, V. Timmerman, F. Hentati and P. De Jonghe, 2003, "Identification of Novel GDAP1 Mutations Causing Autosomal Recessive Charcot-Marie-Tooth Disease", *Neuromuscular Disorders*, Vol. 13, No. 9, pp. 720-728.

Baxter, R. V., K. Ben Othmane, J. M. Rochelle, J. E. Stajich, C. Hulette, S. Dew-Knight, F. Hentati, M. Ben Hamida, S. Bel, J. E. Stenger, J. R. Gilbert and J. M. Vance, 2002, "Ganglioside-induced Differentiation-associated Protein-1 is Mutant in Charcot-Marie-Tooth Disease Type 4A/8q21", *Nature Genetics*, Vol. 30, No. 1, pp. 21-22.

Berman, S. B., F. J. Pineda and J. M. Hardwick, 2008, "Mitochondrial Fission and Fusion Dynamics: The Long and Short of it", *Cell Death and Differentiation*, Vol. 15, No. 7, pp. 1147-1152.

Boerkoel, C. F., H. Takashima, M. Nakagawa, S. Izumo, D. Armstrong, I. Butler, P. Mancias, S. C. Papasozomenos, L. Z. Stern and J. R. Lupski, 2003, "CMT4A: Identification of a Hispanic GDAP1 Founder Mutation", *Annals of Neurology*, Vol. 53, No. 3, pp. 400-405.

Bucci, C., O. Bakke and C. Progida, 2012, "Charcot-Marie-Tooth Disease and Intracellular Traffic", *Progress in Neurobiology*, Vol. 99, No. 3, pp. 191-225.

Cassereau, J., A. Chevrollier, N. Gueguen, V. Desquiret, C. Verny, G. Nicolas, F. Dubas, P. Amati-Bonneau, P. Reynier, D. Bonneau and V. Procaccio, 2011, "Mitochondrial Dysfunction and Pathophysiology of Charcot-Marie-Tooth Disease Involving GDAP1 Mutations", *Experimental Neurology*, Vol. 227, No. 1, pp. 31-41.

Chapman, A. L., E. J. Bennett, T. M. Ramesh, K. J. De Vos and A. J. Grierson, 2013, "Axonal Transport Defects in a Mitofusin 2 Loss of Function Model of Charcot-Marie-Tooth Disease in Zebrafish", *PLoS One*, Vol. 8, No. 6.

Chen, H. and D. C. Chan, 2005, "Emerging Functions of Mammalian Mitochondrial Fusion and Fission", *Human Molecular Genetics*, Vol. 14, No. 2, pp. 283-289.

Chen, H. and D. C. Chan, 2009, "Mitochondrial Dynamics--Fusion, Fission, Movement, and Mitophagy--in Neurodegenerative Diseases", *Human Molecular Genetics*, Vol. 18, No. 2, pp. 169-176.

Cherbas, L., A. Willingham, D. Zhang, L. Yang, Y. Zou, B. D. Eads, J. W. Carlson, J. M. Landolin, P. Kapranov, J. Dumais *et al.*, 2011, "The Transcriptional Diversity of 25 Drosophila Cell Lines", *Genome Research*, Vol. 21, No. 2, pp. 301-314.

Choi, C. M., S. Vilain, M. Langen, S. Van Kelst, N. De Geest, J. Yan, P. Verstreken and B. A. Hassan, 2009, "Conditional Mutagenesis in Drosophila", *Science*, Vol. 324, No. 5923, p. 54.

Clarke, T. F. t. and P. L. Clark, 2008, "Rare Codons Cluster", *PLoS One*, Vol. 3, No. 10.

Crimella, C., A. Tonelli, G. Airoldi, C. Baschirotto, M. G. D'Angelo, S. Bonato, L. Losito, A. Trabacca, N. Bresolin and M. T. Bassi, 2010, "The GST Domain of GDAP1 is a Frequent Target of Mutations in the Dominant Form of Axonal Charcot Marie Tooth Type 2K", *Journal of Medical Genetics*, Vol. 47, No. 10, pp. 712-716.

Cuesta, A., L. Pedrola, T. Sevilla, J. Garcia-Planells, M. J. Chumillas, F. Mayordomo, E. LeGuern, I. Marín, J. J. Vílchez and F. Palau, 2002, "The Gene Encoding Ganglioside-induced Differentiation-associated Protein 1 is Mutated in Axonal Charcot-Marie-Tooth Type 4A Disease", *Nature Genetics*, Vol. 30, No. 1, pp. 22-25.

Detmer, S. A., and D. C. Chan, 2007, "Functions and Dysfunctions of Mitochondrial Dynamics", *Nature Reviews Molecular Cell Biology*, Vol. 8, No. 11, pp. 870-879.

Duffy, J. B., 2002, “GAL4 System in Drosophila: A Fly Geneticist's Swiss Army Knife”, *Genesis*, Vol. 34, No. 1-2, pp. 1-15.

Eaton, D. L., and T. K. Bammler, 1999, “Concise Review of the Glutathione S-transferases and Their Significance to Toxicology”, *Toxicological Sciences*, Vol. 49, No. 2, pp. 156-164.

Fledrich, R., R. M. Stassart and M. W. Sereda, 2012, “Murine Therapeutic Models for Charcot-Marie-Tooth (CMT) Disease”, *British Medical Bulletin*, No. 102, pp. 89-113.

Graveley, B. R., A. N. Brooks, J. W. Carlson, M. O. Duff, J. M. Landolin, L. Yang, C. G. Artieri, M. J. van Baren, N. Boley, B. W. Booth *et al.*, 2011, “The Developmental Transcriptome of Drosophila melanogaster”, *Nature*, Vol. 471, No. 7339, pp. 473-479.

Greenspan, R. J., 2004, *Fly pushing: The Theory and Practice of Drosophila Genetics*, Second edition, Cold Spring Harbor Laboratory Press, Cold Spring Harbor, New York.

Harding, A. E. and P. K. Thomas, 1980, “Genetic Aspects of Hereditary Motor and Sensory Neuropathy (Types I and II)”, *Journal of Medical Genetics*, Vol. 17, No. 5, pp. 329-336.

Laborde, E., 2010, “Glutathione Transferases as Mediators of Signaling Pathways Involved in Cell Proliferation and Cell Death”, *Cell Death and Differentiation*, Vol. 17, No. 9, pp. 1373-1380.

Lloyd, T. E. and J. P. Taylor, 2010, “Flightless Flies: Drosophila Models of Neuromuscular Disease”, *Annals of New York Academy of Sciences*, No. 1184, pp. e1-20.

Low, W. Y., H. L. Ng, C. J. Morton, M. W. Parker, P. Batterham and C. Robin, 2007, “Molecular Evolution of Glutathione S-transferases in the Genus Drosophila”, *Genetics*, Vol. 177, No. 3, pp. 1363-1375.

Lupski, J. R., R. M. de Oca-Luna, S. Slaugenhaupt, L. Pentao, V. Guzzetta, B. J. Trask, O. Saucedo-Cardenas, D. F. Barker, J. M. Killian, C. A. Garcia, A. Chakravarti and P. I.

Patel, 1991, "DNA Duplication Associated with Charcot-Marie-Tooth Disease Type 1A", *Cell*, Vol. 66, No. 2, pp. 219-232.

Marco, A., A. Cuesta, L. Pedrola, F. Palau and I. Marin, 2004, "Evolutionary and Structural Analyses of GDAP1, Involved in Charcot-Marie-Tooth Disease, Characterize a Novel Class of Glutathione Transferase-related Genes", *Molecular Biology and Evolution*, Vol. 21, No. 1, pp. 176-187.

Martyn, C. N. and R. A. Hughes, 1997, "Epidemiology of Peripheral Neuropathy", *Journal of Neurology, Neurosurgery and Psychiatry*, Vol. 62, No. 4, pp. 310-318.

McIlwain, C. C., D. M. Townsend and K. D. Tew, 2006, "Glutathione S-transferase Polymorphisms: Cancer Incidence and Therapy", *Oncogene*, Vol. 25, No. 11, pp. 1639-1648.

Metaxakis, A., S. Oehler, A. Klinakis and C. Savakis, 2005, "Minos as a Genetic and Genomic Tool in Drosophila melanogaster", *Genetics*, Vol. 171, No. 2, pp. 571-581.

Nelis, E., C. Van Broeckhoven, P. De Jonghe, A. Lofgren, A. Vandenberghe, P. Latour, E. Le Guern, A. Brice, M. L. Mostacciuolo, F. Schiavon, *et al*., 1996, "Estimation of the Mutation Frequencies in Charcot-Marie-Tooth Disease Type 1 and Hereditary Neuropathy with Liability to Pressure Palsies: a European Collaborative Study", *European Journal of Human Genetics*, Vol. 4, No. 1, pp. 25-33.

Niemann, A., M. Ruegg, V. La Padula, A. Schenone and U. Suter, 2005, "Ganglioside-induced Differentiation Associated Protein 1 is a Regulator of the Mitochondrial Network: New Implications for Charcot-Marie-Tooth Disease", *Journal of Cell Biology*, Vol. 170, No. 7, pp. 1067-1078.

Niemann, A., K. M. Wagner, M. Ruegg and U. Suter, 2009, "GDAP1 Mutations Differ in Their Effects on Mitochondrial Dynamics and Apoptosis Depending on the Mode of Inheritance", *Neurobiology of Disease*, Vol. 36, No. 3, pp. 509-520.

Noack, R., S. Frede, P. Albrecht, N. Henke, A. Pfeiffer, K. Knoll, T. Dehmel, Z. U. Meyer, G. Hörste and M. Stettner, 2012, "Charcot-Marie-Tooth Disease CMT4A: GDAP1 Increases Cellular Glutathione and the Mitochondrial Membrane Potential", *Human Molecular Genetics*, Vol. 21, No. 1, pp. 150-162.

Pandey, U. B. and C. D. Nichols, 2011, "Human Disease Models in Drosophila melanogaster and the Role of the Fly in Therapeutic Drug Discovery", *Pharmacological Reviews*, Vol. 63, No. 2, pp. 411-436.

Pedrola, L., A. Espert, T. Valdes-Sanchez, M. Sanchez-Piris, E. E. Sirkowski, S. S. Scherer, F. Farinas and F. Palau, 2008, "Cell Expression of GDAP1 in the Nervous System and Pathogenesis of Charcot-Marie-Tooth Type 4A Disease", *Journal of Cellular and Molecular Medicine*, Vol. 12, No. 2, pp. 679-689.

Pedrola, L., A. Espert, X. Wu, R. Claramunt, M. E. Shy and F. Palau, 2005, "GDAP1, the Protein Causing Charcot-Marie-Tooth Disease Type 4A, is Expressed in Neurons and is Associated with Mitochondria", *Human Molecular Genetics*, Vol. 14, No. 8, pp. 1087-1094.

Raza, H., 2011, "Dual Localization of Glutathione S-transferase in the Cytosol and Mitochondria: Implications in Oxidative Stress, Toxicity and Disease", *Federation of European Biochemical Societies Journal*, Vol. 278, No. 22, pp. 4243-4251.

Reiter, L. T., L. Potocki, S. Chien, M. Gribskov and E. Bier, 2001, "A Systematic Analysis of Human Disease-associated Gene Sequences in Drosophila melanogaster", *Genome Research*, Vol. 11, No. 6, pp. 1114-1125.

Senderek, J., C. Bergmann, V. T. Ramaekers, E. Nelis, G. Bernert, A. Makowski, S. Züchner, P. De Jonghe, S. Rudnik-Schöneborn, K. Zerres and J. M. Schröder, 2003, "Mutations in the Ganglioside-induced Differentiation-associated Protein-1 (GDAP1) Gene in Intermediate Type Autosomal Recessive Charcot-Marie-Tooth Neuropathy", *Brain*, Vol. 126, No. 3, pp. 642-649.

Sevilla, T., A. Cuesta, M. J. Chumillas, F. Mayordomo, L. Pedrola, F. Palau and J. Vilchez, 2003, "Clinical, Electrophysiological and Morphological Findings of Charcot-Marie-Tooth Neuropathy with Vocal Cord Palsy and Mutations in the GDAP1 Gene", *Brain*, Vol. 126, No. 9, pp. 2023-2033.

Shield, A. J., T. P. Murray and P. G. Board, 2006, "Functional Characterisation of Ganglioside-induced Differentiation-associated Protein 1 as a Glutathione Transferase", *Biochemical and Biophysical Research Communications*, Vol. 347, No. 4, pp. 859-866.

Siskind, C. E., S. Panchal, C. O. Smith, S. M. Feely, J. C. Dalton, A. B. Schindler and K. M. Krajewski, 2013, "A Review of Genetic Counseling for Charcot Marie Tooth Disease (CMT)", *Journal of Genetic Counseling*, Vol. 22, No. 4, pp. 422-436.

Sivera, R., C. Espinos, J. J. Vilchez, F. Mas, D. Martinez-Rubio, M. J. Chumillas, F. Mayordomo, N. Muelas, L. Bataller, F. Palau and T. Sevilla, 2010, "Phenotypical Features of the p.R120W Mutation in the GDAP1 Gene Causing Autosomal Dominant Charcot-Marie-Tooth Disease", *Journal of the Peripheral Nervous System*, Vol. 15, No. 4, pp. 334-344.

Storkebaum, E., R. Leitao-Goncalves, T. Godenschwege, L. Nangle, M. Mejia, I. Bosmans, T. Ooms, A. Jacobs, P. Van Dijck, X. L. Yang *et al*., 2009, "Dominant Mutations in the Tyrosyl-tRNA Synthetase Gene Recapitulate in Drosophila Features of Human Charcot-Marie-Tooth Neuropathy", *Proceedings of the National Academy of Sciences*, Vol. 106, No. 28, pp. 11782-11787.

Sun, H. D., Y. W. Ru, D. J. Zhang, S. Y. Yin, L. Yin, Y. Y. Xie, Y. F. Guan and S. Q. Liu, 2012, "Proteomic Analysis of Glutathione S-transferase Isoforms in Mouse Liver Mitochondria", *World Journal of Gastroenterology*, Vol. 18, No. 26, pp. 3435-3442.

Vallat, J. M., S. Mathis and B. Funalot, 2013, "The Various Charcot-Marie-Tooth Diseases", *Current Opinion in Neurology*, Vol. 26, No. 5, pp. 473-480.

Warming, S., N. Costantino, D. L. Court, N. A. Jenkins and N. G. Copeland, 2005, "Simple and Highly Efficient BAC Recombineering Using galK Selection", *Nucleic Acids Research*, Vol. 33, No. 4, p. 36.

Yang, J. S., H. J. Nam, M. Seo, S. K. Han, Y. Choi, H. G. Nam, S. J. Lee and S. Kim, 2011, "OASIS: Online Application for the Survival Analysis of Lifespan Assays Performed in Aging Research", *PLoS One*, Vol. 6, No. 8, p. 23525.

Zuchner, S., and J. M. Vance, 2006, "Molecular Genetics of Autosomal-dominant Axonal Charcot-Marie-Tooth Disease", *Neuromolecular Medicine*, Vol. 8, No. 1-2, pp. 63-74.